

ABSTRACT

Title of Thesis: Refrigerant Charge Distribution in Unitary Air-conditioning Units

Tianyue Qiu, Master of Science, 2018

Thesis Directed By: Research Professor Yunho Hwang, Ph. D.
Department of Mechanical Engineering

To address the global warming, reduction of refrigerants charge in HVAC systems is becoming an essential topic. An experimental setup was designed and built for investigating the cyclic degradation performance and the refrigerant charge distribution of a unitary air-conditioning unit. A code tester featuring two parallel ducts was developed to properly control air flows according to the ASHRAE standard test conditions. First, baseline tests were carried out under ASHRAE standard test conditions. System performance was compared to manufacturer's specifications to validate the accuracy of the experimental setup. Second, the transient performance of the unit was analyzed and presented, and the degradation coefficient of the unit was evaluated. Third, an approach of refrigerant charge distribution measurement was

proposed and implemented. Refrigerant R410A charge distribution tests were conducted under steady-state conditions and the results were compared with published results of the refrigerant charge distribution in various types of air-conditioning units. It was concluded that the system charge distribution was significantly influenced by various component combinations and the length of refrigerant copper tubing.

REFRIGERANT CHARGE DISTRIBUTION IN A UNITARY AIR-
CONDITIONING UNIT

by

Tianyue Qiu

Thesis submitted to the Faculty of the Graduate School of the
University of Maryland, College Park, in partial fulfillment
of the requirements for the degree of

Master of Science

2018

Advisory Committee:

Research Professor Yunho Hwang, Chair

Professor Jungho Kim

Professor Bao Yang

© Copyright by

Tianyue Qiu

2018

Dedication

To Lin

Acknowledgements

Two-year graduate study flies, and it is really a wonderful journey and adventure. I would like to thank everyone who has helped, supported, guided me in the pursuit of my master's degree.

First, I would like to express my sincere gratitude to my advisor Dr. Yunho Hwang, for offering the opportunity to be a research assistant in the Center for Environmental Energy Engineering (CEEE), guiding me throughout the challenging research projects, taking care of me in my academic study and daily life. And I would like to give my thanks to Dr. Reinhard Radermacher, for all the support and help he provided to achieve my academic and career goals.

Second, I would like to give my deepest thanks to our lab managers, Mr. Jan Muehlbauer, who taught me basic laboratory skills and provided valuable advice for building experimental test facilities and created a comfortable research environment in CEEE heat pump lab. And I would also like to express my appreciation to my colleagues and friends, Dale Voelker, Lei Gao, Rohit Dhumane, Dr. Jiazhen Ling, Dongyu Chen, Yiyuan Qiao, Joseph Baker, Ellery Klein, David Catalini, Nehemiah Emaikwu, Dr. Xiaojie Lin, Dr. Tao Cao, Zhenyuan Mei, Hanlong Wan, Ransisi Huang, Kaixuan Jiang, Yuanzheng Zhu, and all people I met in the United States, who made this two-year journey unforgettable.

Third, I would like to express my thanks to UTC-CCS colleagues, Jack Esformes, Allen Chad Kirkwood, and Jie Li, who provided financial and technical supports throughout the two-year research project.

Finally, I would like to thank my family, especially my mother, Lin Guan, for supporting and loving me in my pursuit of every life goal for the past twenty-four years.

Table of Contents

Dedication	ii
Acknowledgements.....	iii
List of Tables	viii
List of Figures	ix
Chapter 1: Introduction	1
1.1 Background.....	1
1.2 Objectives	3
Chapter 2: Literature Review	4
2.1 Transient Performance Testing and Modeling of Air-conditioning Units....	4
2.2 Refrigerant Charge Distribution Measurement.....	8
Chapter 3: Experimental Setup	15
3.1 System Schematic Diagram	15
3.1.1 ASHRAE Standard Testing	15
3.1.2 Refrigerant Charge Distribution Measurement.....	16
3.2 Test Conditions and Test Procedure	18
3.2.1 ASHRAE Test Conditions	18
3.2.2 Test Procedure	18
3.3 Split Air-conditioning Unit and Code Tester.....	19
3.4 Expansion System.....	21
3.5 Instrumentation	23
3.5.1 Absolute and Differential Pressure Transducers.....	23

3.5.2	Thermocouple and RTD	24
3.5.3	Refrigerant Mass Flow Meter	26
3.5.4	AC Watt Transducer	28
3.5.5	Dewpoint Sensor	29
3.5.6	Air Damper	30
3.5.7	Quick Closing Valve	31
3.5.8	Recovery Compressor	32
3.5.9	Summary	33
3.6	Data Acquisition System	34
3.7	Uncertainty Analysis	36
Chapter 4: Test Results and Data Analysis		39
4.1	Steady-state Condition Baseline Test	39
4.1.1	Charge Calibration	39
4.1.2	Data Summary (ASHRAE A, B, and C Tests)	40
4.2	Cyclic Condition Test	46
4.2.1	Data Summary (ASHRAE D Test)	46
4.2.2	Evaluation of the Degradation Coefficient	55
4.2.3	Effect of Thermal Mass of the Code Tester	58
4.3	Refrigerant Charge Distribution Tests	60
4.3.1	Internal Volume Calibration	60
4.3.2	Charge Sensitivity Test	63
4.3.3	Oil Monitoring	66

4.3.4	Charge Distribution Test Results	68
4.3.5	Results Comparison with Published Data.....	72
Chpater 5:	Conclusions	76
Chpater 6:	Future Work	78
Reference	81

List of Tables

Table 1: ASHRAE Test Conditions for Cooling Mode of Units Having a Single-speed Compressor	18
Table 2: Specification of Installed Instrumentations	34
Table 3: Systematic Uncertainties of Direct-measured Variables	38
Table 4: Charge Calibration under Steady-state Conditions.....	39
Table 5: Validation of Extra System Charge	40
Table 6: Data Summary of ASHRAE A Condition Test	41
Table 7: Data Summary of ASHRAE B Condition Test	42
Table 8: Data Summary of ASHRAE C Condition Test	43
Table 9: Evaluation of Degradation Coefficient of Five Cyclic Tests.....	57
Table 10: Internal Volume Measurement for Outdoor Unit Section	61
Table 11: Internal Volume Measurement for Indoor Unit plus Vapor Line Section..	62
Table 12: Internal Volume Measurement for Liquid Line Section.....	62
Table 13: Refrigerant Charge Distribution under Steady-state Conditions	69
Table 14: Published Experimental Results of Refrigerant Charge Distribution.....	73

List of Figures

Figure 1: Estimates for the Global A/C Market by Region, by Volume as Calculated by Building Service Research Information Association (BSRIA) [2].....	1
Figure 2: System Schematic Diagram of ASHRAE Standard Testing.....	15
Figure 3: Modified System Schematic Diagram with an Expansion System	17
Figure 4: Code Tester with a Bypass Duct	20
Figure 5: Expansion System for Charge Distribution Measurement	21
Figure 6: Heat Exchanger with 24V DC Fan.....	22
Figure 7: Refrigerant-side Absolute and Differential Pressure Transducers	23
Figure 8: Air-side Barometric and Differential Pressure Transducers	24
Figure 9: OMEGA T-Type Thermocouple with Sheath.....	25
Figure 10: Emerson Micromotion 2700 Mass Flow Meter	26
Figure 11: Ohio Semitronics AC Watt Transducer.....	28
Figure 12: Overview of the Electric Box and the Variac for Outdoor Unit Power Supply	29
Figure 13: DewTrak II Dewpoint Sensor.....	30
Figure 14: Air Damper with Electrical Actuator	30
Figure 15: Assured-Automation Quick Closing Valve.....	31
Figure 16: Electrical Box to Control the Recovery Compressor	32
Figure 17: NI Data Acquisition Modules of the Code Tester	34
Figure 18: NI Data Acquisition Modules of the Outdoor Unit.....	35

Figure 19: Data Visualization Window in LabVIEW Program.....	36
Figure 20: Refrigerant Temperature versus Time under Cyclic Condition	47
Figure 21: Refrigerant Temperature Map during Start-up.....	48
Figure 22: Air Entering and Leaving Temperature of Indoor Unit under Cyclic Condition.....	49
Figure 23: Refrigerant Pressure under Cyclic Condition.....	50
Figure 24: Refrigerant Pressure Map during Start-up.....	51
Figure 25: Refrigerant Differential Pressure across Components during Cyclic Condition.....	52
Figure 26: Outdoor Unit Power Consumption and Refrigerant Mass Flow Rate during Cyclic Condition	53
Figure 27: Cooling Capacity during Cyclic Condition	54
Figure 28: Cooling Capacity Comparison under the Cyclic Condition	58
Figure 29: Correlations between Subcooling and Condensing Pressure with System Charge	64
Figure 30: Correlations between Outdoor Unit Power Consumption with System Charge	65
Figure 31: The Scroll Compressor with a Sight Tube	66
Figure 32: Compressor Oil Level under UV Light.....	67
Figure 33: Oil Level under UV Light before (Left) and after One Charge Distribution Test (Right)	68

Figure 34: Vapor Pressure Correlation with Temperature of R410A and POE 32 Oil [35].....	70
Figure 35: Charge Distribution of Steady-state Conditions Breakdown of Sections .	71
Figure 36: Refrigerant Charge Distribution under ASHRAE A Condition.....	73
Figure 37: Refrigerant Charge Distribution under ASHRAE C Condition.....	74
Figure 38: Refrigerant Charge Distribution under ASHRAE A Condition (Liquid Line Length Corrected).....	75
Figure 39: Refrigerant Charge Distribution under ASHRAE C Condition (Liquid Line Length Corrected).....	75

Nomenclature

\dot{Q}_{air}	Total air-side cooling capacity [W]
\dot{Q}_{sen}	Air-side sensible cooling capacity [W]
\dot{Q}_{lat}	Air-side latent cooling capacity [W]
\dot{Q}_{mi}	Measured indoor airflow [W]
\bar{c}_p	Average specific heat of air blowing through IDU [J/(kg•K)]
t_{a1}	Temperature of the air entering IDU [°C]
t_{a2}	Temperature of the air leaving IDU [°C]
v_n	Specific volume of dry air entering IDU [m ³ /kg]
W_1	Humidity ratio of air entering IDU [kg/kg]
W_2	Humidity ratio of air leaving IDU [kg/kg]
h_{fg}	Latent heat of vaporization [kJ/kg]
\dot{Q}_{ref}	Refrigerant-side cooling capacity [W]
h_{r1}	Enthalpy of refrigerant entering evaporator [kJ/kg]
h_{r2}	Enthalpy of refrigerant leaving evaporator [kJ/kg]
P_{df}	Default fan power of commercial indoor unit [W]
P_{ODU}	ODU power consumption [W]
C_d	Degradation Coefficient
EER_{cyc}	Energy efficient ratio under cyclic condition
EER_{ss}	Energy efficient ratio under steady-state condition

CLF	Cooling load factor
\dot{q}_{tci}	Indoor air-side total cooling capacity [Btu/h]
\dot{E}_t	Total power input [W]
q_{cyc}	Indoor air-side total integrated capacity during cyclic operation [Btu]
E_{cyc}	Total power input during cyclic operation consisting of one compressor ON and one compressor OFF period [W*h]
t_{cyc}	Duration of time for one complete cycle consisting of one compressor ON time and one compressor OFF time [h]

List of Abbreviation

AC	Air Conditioning
AHRI	Air Conditioning Heating & Refrigeration Institute
ASHRAE	American Society of Heating, Refrigerating and Air-Conditioning Engineers
CLF	Cooling Load Factor
COP	Coefficient of Performance
DAQ	Data Acquisition
EB	Energy Balance
EER	Energy Efficiency Ratio
EEV	Electronic Expansion Valve
GWP	Global Warming Potential
HVAC&R	Heating, Ventilation, Air Conditioning & Refrigeration
IDU	Indoor Unit

IV	Internal Volume
LLM	Liquid Level Method
LNМ	Liquid Nitrogen Method
NI	National Instruments
OD	Outer Diameter
ODU	Outdoor Unit
OMF	Oil Mass Fraction
PVC	Polyvinyl Chloride
QLNM	Quasi Liquid Nitrogen Method
QOMM	Quasi Online Measurement Method
RTD	Resistance Temperature Detector
SEER	Seasonal Energy Efficiency Ratio
STHAC	Split Type Household Air Conditioner
TEV (TXV)	Thermal Expansion Valve
UMCP	University of Maryland, College Park
VCC	Vapor Compressor Cycle

Chapter 1 : Introduction

1.1 Background

Energy is one the most essential factor influencing the development of the human society. For energy market, the global air conditioner stock is expected to increase from 660 million units in 2015 to more than 1.5 billion units by 2030 [1]. The trend of estimated packaged air-conditioning units installed worldwide is shown in the Figure 1 [2]. As estimated in 2013, the total packaged air-conditioning unit could exceed 120 million worldwide in 2017 and this number keeps increasing with time. Moreover, it is quite a reasonable number if compared to the world total population since most regions of the world need air-conditioning systems and some regions even have more than one unit per household. Therefore, the energy efficiency study related to HVAC&R systems



Figure 1: Estimates for the Global A/C Market by Region, by Volume as Calculated by Building Service Research Information Association (BSRIA) [2]

is quite essential to human society. Residential HVAC&R systems, including air conditioners, heat pumps and refrigerators, experience frequent on-and-off cycles to maintain space condition to set-points. In most daily conditions, the system may not run at full capacity since it is common to oversize the system to meet the peak load. Considering the start-up of an air-conditioning (AC) system, it typically requires higher compressor power input than that during steady-state operation to overcome the static mechanical friction and delivers lower capacity than that during steady-state operation. This inevitably leads to a performance degradation of the AC system. One important reason is that, in the start-up, the refrigerant flow has to overcome a certain amount of system's thermal inertia. Take the example of an evaporator: its tube wall temperature may be in equilibrium with room air during off-cycle period. Once the compressor turns on, the cooling capacity of cold refrigerant has to be used for reducing the tube wall temperature before room air can then reject heat to the evaporator. During this wall-cooling period which may last minutes, the evaporator capacity delivered to the space is essentially negligible due to a very small temperature difference between air and tube wall. Furthermore, depending on the expansion device, during OFF time, the refrigerant charge tends to migrate to the evaporator, while during steady-state operation the majority of the charge will migrate to the condenser side. The need for refrigerant migration severely limits evaporator performance at startup and can lead to compressor flooding. Therefore, it is important to introduce cyclic degradation into the seasonal energy efficiency ratio (SEER) calculation in addition to steady-state performance data.

1.2 Objectives

The first goal of this study is to investigate variables that have effects on the degradation coefficient of unitary residential air-conditioning units. To achieve this, a code tester which has the capability for cyclic test needs to be built. Since the code tester and the psychrometric chamber are in different rooms, refrigerant piping has to go through the wall and connecting the indoor and outdoor units. Due to the slow ramping up and long response time of controlling air temperature circulating in the code tester, air temperature and relative humidity is set to test condition and air is kept running all the time during the cyclic test. To mimic the actual operation of unit under ON/OFF condition, in addition to the ON/OFF of the compressor, a bypass duct parallel to the testing duct in which the indoor unit is installed needs to be built. With respect to testing, first, tests under steady-state condition (ASHRAE A, B, and C conditions) needs to be carried out. Second, cyclic test under ASHRAE D condition needs to be conducted and degradation coefficient is evaluated based on the cyclic test data. Variables including thermal inertia of the code tester need to be identified and the test facility needs to be modified accordingly to study the effects of those variables on the cyclic performance of the system. In addition to the study of degradation coefficient, the second goal of this study is to measure refrigerant charge distribution. Expansion method is proposed to measure the refrigerant charge inside system components. To implement this approach, quick closing valves need to be installed along the refrigerant loop and expansion tanks need to be set up for each system section. Moreover, the refrigerant charge distribution measured is compared with published results.

Chapter 2 : Literature Review

2.1 Transient Performance Testing and Modeling of Air-conditioning Units

Hwang et al. (1998) [3] performed experiments to investigate the transient characteristics during speeding up of an inverter heat pump. The results show that the main cause of the transient phenomena is due to the excessive refrigerant into compressor from increased refrigerant mass flow rate and suction pressure drop. The migration of liquid state refrigerant was the most important factor in determining the accuracy for an experimental result or development of transient model. And they developed transient model for each major component, and the results of the simulation were in good agreement with the experimental ones within 10%.

Kim et al. (2000) [4] presented experimental results on the shut-down and start-up characteristics of a residential split air-conditioning system. The pressure of the system after shut-down equalizes within three minutes and increases gradually due to heat exchange with environment before reaching the pressure of steady state. The refrigerant in the evaporator exists in saturated state while the refrigerant in the condenser is at superheated state after shut-down. For 30 seconds after start-up, the performance degradation of the system is mainly due to latent heat transfer since additional condensate evaporation from the coil surface into the environment. The performance degradation due to refrigerant migration and thermal mass can be reduced when smaller refrigerant charge and weight heat exchangers are used.

Kapadia et al. (2009) [5] built a dynamic model for studying the transient characteristics of a split air-conditioner during start-up using MATLAB platform. The temperature produced by the model was validated by tests on a split air-conditioning unit, and the pressure response was validated by published experimental data. The results show that the total transient loss during start-up was found to be 18.5% for the R410A and 18.7% for the R22 system.

Wu et al. (2015) [6] experimentally investigated the cold start-up characteristics of a rotary compressor in a R290 air-conditioning system under cooling condition. The time from start-up to steady state of R290 was much longer than those of R22 and R410A systems. A slight liquid slugging was found at the initial time during start-up process in the R290 rotary compressor. However, the pressures rapidly decreased after reaching the maximum value during the start-up process. At the initial time after startup, the cylinder temperature decreased as the suction temperature sharply decreased, while the motor stator temperature and the muffler temperature increased rapidly. The mixture of oil and refrigerant viscosity reached steady state value of 4 cp after 500 seconds after a short decrease to 1.33 cp. The maximum and stable value of solubility was 42% in 250 seconds and 21% in 500 seconds, respectively.

Li and Alleyne (2009) [7] developed a switched modeling approach to describe the transient behaviors in heat exchangers during compressor shut-down and start-up operations. Switched model representations (five modes for condenser and two modes for evaporator) were adopted to develop a new moving-boundary heat exchanger, which can capture the transient behaviors for VCC systems.

Kærn et al. (2011) [8] developed a numerical model by which they performed a generic investigation by means of controlling the superheat in the evaporator channels for residential air-conditioning unit. System performance in terms of cooling capacity and COP increases 5.0% by implementing the compensation method. And better performance is expected when upgrading the evaporator capacity.

Bagarella et al. (2013) [9] investigated the cycling losses of a 6.8 kW water-to-air chiller. Values of EER of cycling condition and steady-state condition were compared. Up to 13% cyclic losses with a penalty increase for low load factors. And they installed solenoid valves in series with the TEV, by which they obtained a better behavior when load factor fell below 30%. Finally, a chiller equipped with an EEV was investigated to have best performance of keeping the losses below 6% for all experimented load factors.

Wu et al. (2017) [10] experimentally investigated the dynamic characteristic of a R290 rotary compressor and corresponding air conditioner during warm start-up under cooling condition. Test results show that the minimum suction pressure and temperature during the warm start-up is greater than that of the cold start-up, while the maximum discharge pressure during the pressure jump during warm start-up is much lower than that of cold start-up. In addition, they pointed out that the warm start-up was beneficial to the lubrication of bearings due to its relatively higher viscosity of refrigerant/oil mixture in the oil sump.

Cremaschi et al. (2005) [11] parametrically studied the oil retention physics of refrigerant R22, R410A and R134a with miscible and immiscible lubricants. Results

show that oil retention volume is proportional to the oil mass fraction (OMF) of the refrigerant/oil mixture, and suction line is the most critical component for oil retention due to its highest liquid film viscosity and low inertia force from the vapor refrigerant core. Optimized pipe diameter and horizontal pipe line had positive effects on oil retention.

Fuentes et al. (2016) [12] presented a study of the partial load performance of a water-to-water heat pump under different water inertia scenarios. And a theoretical equation was derived for the degradation coefficient (C_d), which pointed out the storage volume as the only effective factor for reducing the degradation effects during start-up. And modified partial load factor equation was proposed to better predict the partial load degradation below certain inertia levels.

Corberan et al. (2013) [13] experimentally investigated the cyclic degradation of a water-to-water refrigeration/heat-pump unit under ON/OFF operation. Results show that the dynamic performance of the heat pump is almost quasi-steady, and negligible start-up period time and losses were observed. The main cause of stand-by losses is the consumption of the electronics.

Wang and Wu (1989) [14] reported that the refrigerant migration during shut-down period had a great influence on the start-up transient performance. And energy losses could be reduced by preventing the refrigerant from migrating during shut-down. Specifically, the motor power during start-up decreased by 4%, the peak value reduces by 9.4% and the evaporating temperature decreases rapidly as results of adding a

magnetic shut-off valve which was closed on compressor shut-down. In addition, the heat inertia should be as small as possible to minimize transient losses.

Tassou and Votsis (1992) [15] experimentally investigated the transient response of an domestic size air-to-water heat pump system during start-up conditions. As a result, the transient characteristics of a heat pump system depend not only on the thermal mass of its components but also on the migration of refrigerant from the condenser to the evaporator during the off-cycle. ON/OFF cycling losses associated with refrigerant migration could be reduced from 11% to 6% by implementing flow controls preventing refrigerant migration during OFF cycle.

2.2 Refrigerant Charge Distribution Measurement

As investigated in the open literature, the refrigerant migration during cyclic conditions is an essential factor in determining the transient losses of HVAC systems. Therefore, the experimental investigation on refrigerant migration under cyclic conditions of a split residential air-conditioning unit is proposed for this study.

Mulroy and Didion (1985) [16] investigated the relationship between cyclic refrigerant migration and cyclic loss for a residential air conditioner. The refrigerant migration was measured at different points in the cyclic operation by simultaneously shutting off the pneumatic valves. The unit performance was compared to single and double time constant regressive approximations and to the time constant calculated from the evaporator mass and heat transfer coefficients. In addition, complex and burdensome

tests were required by ASHRAE Standard 116 to validate the transient model, by which the cyclic operation of any given air conditioner could be characterized.

Belth et al. (1988) [17] experimentally investigated the change in mass of each component of a residential heat pump or air-conditioning in a transient mode. Single and two balanced beam methods were implemented together with mass flow rate measurement to obtain the refrigerant mass data continuously. One problem was that much greater refrigerant charge was required by the zig-zag tubes designed to realize the balanced-beam mass measurement method when compared the normal system charge.

Sheth and Newell (2005) [18] experimentally studied the oil entrapment data in different components of a commercial air-conditioning system using refrigerant R-22 and compared the test data with the refrigerant charge and oil holdup predictions. Overall, the predicted refrigerant mass quantities were approximately within 20% of the experimental data collected, while the predicted oil mass differed greatly from the experimental data for both the evaporator and the condenser.

Bjork and Palm (2005) [19] investigated the refrigerant charge distribution in a cycling domestic refrigerator using isobutane during start-up and shut-down. Expansion method was implemented to measure the refrigerant mass. Results show that four types of losses are acknowledged due to the ON/OFF cycling. In total, the efficiency and capacity were reduced by 9% and 11%, respectively. In addition, notwithstanding the limitation of the study in terms of the tested subject, the possibilities to increase

efficiency during cyclic conditions by implementing the refrigerant-migration-preventing methods during OFF period were brought up for discussion.

Poggi et al. (2007) [20] presented a review of the refrigerant charge studies including methodologies of charge measurement, void fraction correlations and evaluated the influence of refrigerant charge on the coefficient of performance (COP) and the cooling capacity, and finally inventoried means to minimize the refrigerant charge. First, quick-closing-valve technique and on-line measurement were reported as two main categories in refrigerant charge measurement. Second, charge reduction options were proposed as follows: a) use of refrigerant systems with secondary refrigeration, b) use of direct expansion fed evaporator, c) use of natural refrigerant such as hydrocarbon, ammonia or CO₂, and d) use of compact heat exchangers.

Peuker and Hrnjak (2008) [21] presented a comparison between the start-up characteristics for an automotive R744 and an automotive R134a air-conditioning systems. One correlation could describe the cooling capacities for both systems. Quick-closing-valve with liquid nitrogen method was implemented to measure the refrigerant charge for R134a system. From the test data of R134a system, it was found that 28% of compressor power input could be saved by preventing the migration of refrigerant before start-up. The uncertainty for how much refrigerant is in one section is less 2%. In addition, majority of oil migration happening between the compressor and accumulator was studied.

Ding et al. (2008) [22] presented methods for measuring the refrigerant mass distribution inside refrigerant systems. The quasi on-line measurement method

(QOMM) was implemented for measuring the refrigerant mass inside heat exchangers, which could avoid refrigerant waste and accelerate the measurement process. Meanwhile, QOMM together with oil level observation method was adopted for the measurement inside compressor and liquid level method (LLM) was used to measure the refrigerant mass inside the accumulator and the receiver. The results show that the sum of measured refrigerant mass in all components has a maximum deviation of 1.7% from previously known refrigerant charge inventory.

Li et al. (2011) [23, 24] developed a dynamic model of a R134a automotive air-conditioning system to capture the refrigerant migration during compressor shut-down and start-up operations. Results show that the system model was able to well predict the refrigerant mass migration during the shut-down and the start-up period, with the errors between 4% and 8%. It was anticipated that the mass migration prediction errors would remain on the order of 10% or less for other similar scenarios including cases of variation of liquid tube length and ramping compressor speed.

Palmiter et al. (2011) [25] experimentally studied the effects of improper airflow and refrigerant charge on the seasonal performance of a 10.6 kW R410A residential heat pump with a thermostatic expansion valve (TXV). Six climate zones were tested with system variations of 75%, 100% and 125% of nominal refrigerant charge and 75% and 100% of rated airflow. Results show that the heating and cooling COP increased with the increasing system charge for given airflow rate and reduced with the decreasing airflow rate.

Li et al. (2015) [26] experimentally investigated the refrigerant mass distribution within a split air conditioner using R290 as refrigerant. Liquid nitrogen method (LNM) was implemented to obtain the refrigerant mass inside components as well as the variance of distribution with changing temperature and compressor speed. Results show that the refrigerant would migrate from condenser to evaporator in heating mode as ambient temperature decreased, while the operating temperature had little effects on the distribution in cooling mode. In addition, the refrigerant that initially had lower temperature flowed out from the heat exchanger into the compressor, accumulator and heat exchanger at higher temperature within first 30s of start-up. And the charge in the heat exchangers gradually increased to stable value while that in the compressor and accumulator reduced after 2 min.

Tang et al. (2016) [27] presented a new quasi-liquid nitrogen method in order to investigate the refrigerant distribution in a R290 split type household air conditioner (STHAC) and the leaking rate under various conditions were conducted. Results show that the maximum deviation of quasi-liquid nitrogen method (QLNM) is 5.29%. Majority of the refrigerant is distributed in the heat exchangers in cooling mode and the portion of mass in the heat exchangers increased with system charge, while the those in other components remained almost the same. High flammable risk was predicted for the indoor unit in cooling mode due to the refrigerant migration from the condenser to the evaporator side during OFF period. In addition, installing a solenoid valve near the capillary tube is experimentally proved to effectively reduce the leaking rate of R290 STHACs.

Jin and Hrnjak (2016) [28] developed a semi-empirical model to predict refrigerant and lubricant inventory in both microchannel condenser and plate-and-fin evaporator of an automotive air-conditioning system. Test data of R134a with PAG46 and R1234yf with PAG46 were used to validate the model. Results show that both the refrigerant and lubricant mass retention in the evaporator and the refrigerant in condenser could be predicted within 20% and 15% errors, respectively. Nevertheless, the oil retention in condenser was always under-predicted unless adding a hypothesis that bottom channels at lower temperature were filled with oil rich liquid. Resulting from the modification, the oil mass in the condenser could be modeled within 15% error.

Liang and Li (2017) [29] developed a system-level finite-volume dynamic model by adopting dynamic lubricant solubility and absorption rate, finite-volume integrated with geometry configuration and fin equivalent simplifications. Results show that reasonable charge, greater displacement and large volume ratio of condenser to evaporator will be beneficial for improving system stability during start-up.

Li et al. (2017) [30] experimentally investigated the refrigerant migration during the start-up and shut-down of a R410A split air conditioner. Quick-closing-valve method was implemented to measure the refrigerant mass inside components. Results demonstrate that the refrigerant distribution rapidly changed with the first 300s of start-up and the first 60s of shut-down operation. Control strategies including increasing the refrigerant charge in condenser and eliminating air rebounds could increase the transient performance during start-up period.

It can be concluded from the literature review that the studies on transient characteristics of split air-conditioning unit using R410A as refrigerant consisting of thermal expansion valve, a scroll compressor and enhanced fin-and-tube heat exchange coils are limited. And there are few papers focusing on the refrigerant charge migration during cyclic condition required by ASHRAE Standard 116. These two aspects are further investigated in this study. Moreover, methods implemented in the open literature to measure the refrigerant mass inside system components are either too complex in terms of equipment and procedure or too vulnerable with respect to measurement accuracy. A modified expansion method is proposed to measure the refrigerant charge inside system components during standard testing conditions.

Chapter 3 : Experimental Setup

3.1 System Schematic Diagram

3.1.1 ASHRAE Standard Testing

To conduct air-conditioning unit testing in accordance with ASHRAE Standard 116 [31] and AHRI Standard 210-240 [32], the test facility is proposed as shown in the Figure 2.

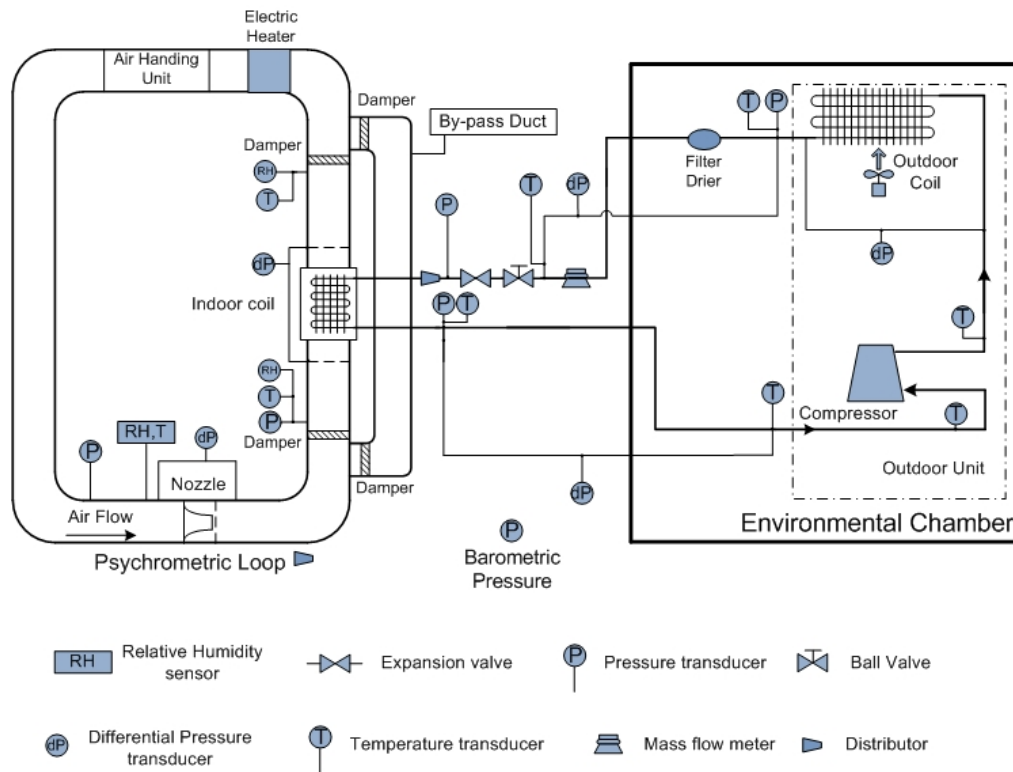


Figure 2: System Schematic Diagram of ASHRAE Standard Testing

The indoor and outdoor units of the split air-conditioning unit were installed in a code tester and a psychrometric chamber, respectively in separate rooms. Copper tubing was brazed to connecting those two heat exchanger coils. As for the code tester, it was

designed and built in accordance with ASHRAE and AHRI standards and equipped with an air handling unit which can control the circulating air temperature and humidity to set points. ASHRAE standard nozzle was installed to measure the airflow rate in the code tester. As for the psychrometric chamber, it can control its temperature and humidity to any setting point in the temperature range of 5-50°C and relative humidity range of 0-100%. The outdoor unit consists of a condenser coil, a scroll compressor and a fan. Thermocouple, absolute and differential pressure, relative humidity and dewpoint transducer were installed at essential locations of both air-side and refrigerant-side. To simulate the cyclic condition, a bypass duct was built parallel to the testing duct in the code tester. The airflow would go through the bypass duct during OFF period and through the testing duct during ON period. And four electrical air dampers were installed to control the airflow. Last but not the least, with additional differential pressure transducers along the refrigerant loop, we can get the pressure distribution map of the whole loop under transient condition, which will provide essential information of transient performance of the system.

3.1.2 Refrigerant Charge Distribution Measurement

Test facility was modified to achieve the objective of investigating refrigerant charge distribution during steady-state conditions as shown in Figure 3. The schematic diagram of the code tester part is not presented in this diagram, which remains the same as before. Three quick closing valves were installed along the refrigerant loop, which can be triggered simultaneously during test to separate the refrigerant loop into three

sections: outdoor unit section, liquid line section, and indoor unit plus vapor line section. Totally, six expansion tanks were set up for refrigerant expansion, and two for each section, which are calculated to be large enough in volumes to guarantee all the refrigerant inside components could be expanded to superheated vapor phase. Thermocouple and an absolute pressure transducer were installed for each section, by which the refrigerant mass can be calculated based on the vapor refrigerant density $\rho(P, T)$ and pre-calibrated internal volume of each section. And three air-to-refrigerant heat exchangers equipped with fans were installed for three sections. In addition, a recovery compressor was installed to pump all the expanded vapor refrigerant back to the system after every expansion process.

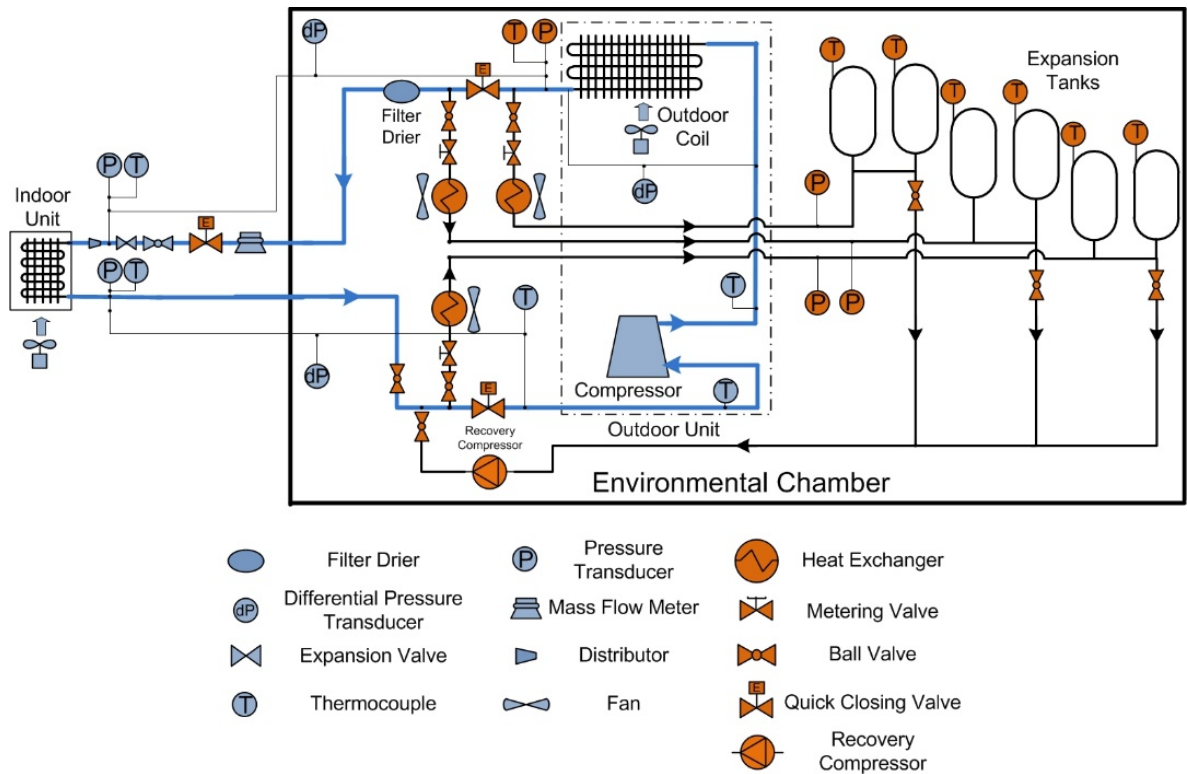


Figure 3: Modified System Schematic Diagram with an Expansion System

3.2 Test Conditions and Test Procedure

3.2.1 ASHRAE Test Conditions

Test conditions were chosen according to ASHRAE Standard 116 [31] and AHRI Standard 210-240 [32] for cooling mode testing of air conditioner with a single-speed compressor. And test matrix is shown in Table 1.

Table 1: ASHRAE Test Conditions for Cooling Mode of Units Having a Single-speed Compressor

	Air Entering IDU		Air Entering ODU	
	Dry Bulb (°C)	Wet Bulb (°C)	Dry Bulb (°C)	Wet Bulb (°C)
ASHRAE A (S.S. Wet)	26.7	19.4	35	23.9
ASHRAE B (S.S. Wet)	26.7	19.4	27.8	18.3
ASHRAE C (S.S. Dry)	26.7	≤13.9	27.8	-
ASHRAE D (Cyclic, Dry)	26.7	≤13.9	27.8	-

Both baseline tests and charge distribution tests were carried out under above conditions. And data from manufacturer was available to validate the repeatability of the system performance.

3.2.2 Test Procedure

Baseline and cyclic tests were carried out while following the standard procedure to test air-conditioning unit and degradation coefficient (C_d) was calculated in accordance with ASHRAE Standard 116.

As for the measurement of charge distribution, test procedure is proposed as follows:

- 1) Run the system under ASHRAE steady-state conditions (A, B or C);
- 2) Stop the compressor at the same time isolate the system into three sections by closing quick closing valves;
- 3) Open releasing valves to expand all the refrigerant into expansion tanks;
- 4) Calculate vapor-phase refrigerant density and mass based on the pre-calibrated internal volumes after expansion process getting stable;
- 5) Run recovery compressor to pump all the refrigerant vapors back to the system.

Basically, above test procedure was repeated for each steady-state condition to make sure the repeatability of the test results.

To achieve the goal of obtaining refrigerant mass distribution, two pre-tests need to be carried out before the charge distribution test. First, internal volumes of three test sections with expansion tanks need to be calibrated. R134a was used instead of R410A to calibrate the internal volume by the same approach of vapor expansion. Second, a charge sensitivity test needs to be carried out to obtain the correlations between system charge and performance parameters including condenser outlet subcooling, condensing pressure, and power consumption. This pre-test is of importance to guarantee the system having the same performance after every expansion process.

3.3 Split Air-conditioning Unit and Code Tester

The unit installed to be tested was a 5-kW split residential air-conditioning unit, which has a single-speed scroll compressor, a thermal expansion valve and enhanced fin-and-

tube heat exchanger coils. The indoor unit and outdoor unit are installed in the code tester and the psychrometric chamber, respectively, both of which can be controlled to setting temperature and relative humidity in accordance with the standard testing conditions.

A code tester was designed and built as shown in Figure 4. To mimic the airflow during ON/OFF cycling and keep air handling unit running, a bypass duct was built parallel to the testing duct. When switching from On to OFF cycle, four air dampers, which were installed at the inlet and outlet of those two ducts respectively, were actuated electrically to bypass the airflow so as to guarantee no air blowing through the evaporator coil during OFF period.

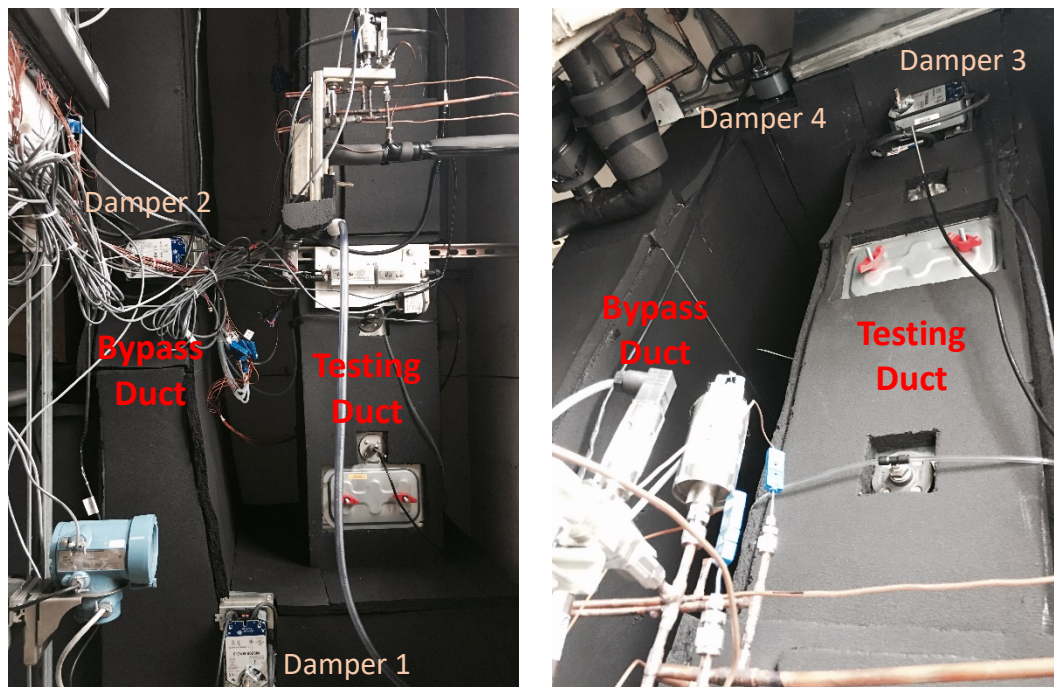


Figure 4: Code Tester with a Bypass Duct

A 0.152 m (6 in.) diameter ASHRAE nozzle and an air-sampling device were installed in the entering section before the indoor unit to measure the circulating airflow rate. And the height of testing duct was design to meet the requirement of ASHRAE Standard 37 [33], which can guarantee accurate pressure measurement. Most of the duct pieces were insulated using one-inch rubber foam insulation made of Buna-N/PVC to minimize the heat exchange between the circulating air with the ambient air. As limitation of space, those two parallel ducts were designed in different cross-section geometries due to the limitation of room space to accommodate the required airflow rate.

3.4 Expansion System

The expansion system was built to measure the refrigerant charge distribution under steady-state conditions shown in Figure 5.

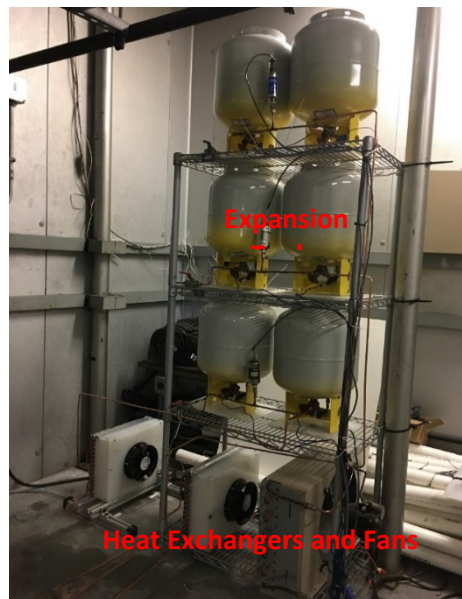


Figure 5: Expansion System for Charge Distribution Measurement

Totally six expansion tanks were set up in the same psychrometric chamber with the outdoor unit, and each tank has an internal volume of 21.6 L, which can ensure all the refrigerants would be expanded to superheated vapor phase. To speed up the expansion process, a heat exchanger with a fan as shown in Figure 6 were installed for each system section. In addition, the shelves of those six tanks were located higher than the unit, which could minimize the oil trapped in the tanks during the expansion process, while the piping from the unit to expansion tanks was the lowest point of the system. Therefore, oil recovery by liquid refrigerant flushing was proposed in case any significant loss of oil in the compressor were observed, in which the liquid refrigerant coming out of condenser will be sent through piping of expansion system and circulate back to the system to recover as much oil as possible. The challenge in this task is that the extra length of expansion piping would require a much larger amount of system



Figure 6: Heat Exchanger with 24V DC Fan

charge. In order to flush with liquid refrigerant, we need to keep sufficient subcooling at condenser outlet. One solution to address the issue is to lower the psychrometric chamber temperature to minimize the heat gain from the chamber air and flush the system in a short time duration.

3.5 Instrumentation

3.5.1 Absolute and Differential Pressure Transducers

Absolute pressure and differential pressure transducers were installed along the refrigerant loop to obtain an accurate refrigerant pressure profile, which would be valuable data source for the validation of transient model for air-conditioning unit in the future study. Especially, absolute pressure transducers were installed at essential locations including the evaporator and condenser outlets for superheat, subcooling and capacity calculation. Absolute pressure was measured by SETRA model 280 and differential pressure was measured by OMEGA PX419 and SETRA model 230, which are shown in Figure 7.



Figure 7: Refrigerant-side Absolute and Differential Pressure Transducers



Figure 8: Air-side Barometric and Differential Pressure Transducers

As for air-side pressures, the air-side differential pressure across the ASHRAE nozzle and indoor unit were measured by SETRA model 264, and barometric pressure transducer of SETRA model 278 was installed to obtain the room ambient pressure.

The pictures of these two models are shown in Figure 8.

All the pressure transducers were calibrated with an OMEGA pressure calibrator model PCL 5000 and linear coefficients were entered in the data acquisition system for recording the corrected pressure values.

3.5.2 Thermocouple and RTD

Thermocouples were installed both on refrigerant side and air side for temperature measurement. For refrigerant-side temperatures, OMEGA T-type thermocouples with



Figure 9: OMEGA T-Type Thermocouple with Sheath

sheath as shown in Figure 9 were installed at condenser outlet, TXV inlet, evaporator outlet and compressor suction. And T-type thermocouple with soldered joint ones were attached to the refrigerant piping surface at compressor discharge, condenser inlet evaporator coil inlet and TXV equilibrium bulb. In addition, soldered joint ones were also installed at compressor oil sump, lower surface and top surface to monitor the operating temperature of the compressor. As for air-side temperatures, thermocouple grids were built to produce more accurate temperature data considering the effect of the maldistribution of the airflow in the code tester. Thermocouple grids of nine thermocouples were installed both at the inlet and outlet of the testing duct, in which the indoor unit was installed, as well as at the inlet of the ASHRAE nozzle. And grid with four thermocouples were installed at the inlet and outlet of the outdoor unit. In addition, T-type thermocouples with sheath were installed in the six expansion tanks

for more accurate refrigerant density calculation due to the air stratification in the psychrometric chamber.

OMEGA 1/10DIN RTD was installed at the inlet of the ASHRAE nozzle to obtain more accurate temperature data by using only thermocouple grid. However, sampling device was installed to pump sampled air out of the duct section for RTD measuring, which has the advantage of more accurate temperature reading but the disadvantage of slow response.

All the thermocouple and RTD were calibrated in the thermostat bath in the lab and linear coefficients are entered in the data acquisition system to record the corrected value.

3.5.3 Refrigerant Mass Flow Meter

Mass flow rate of refrigerant R410A was measured by Emerson Micromotion 2700 Coriolis Mass Flow Meter, which was calibrated in the lab to a customized range of 0-50 g/s as shown in Figure 10. The mass flow meter has a display monitor on which

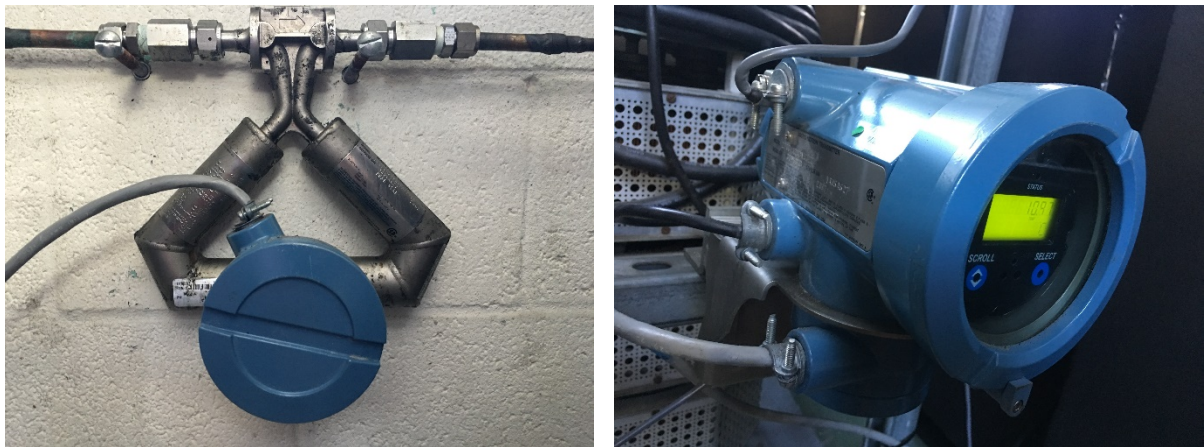


Figure 10: Emerson Micromotion 2700 Mass Flow Meter

users could modify settings and read measured parameters including mass flow rate, fluid density and so on.

The mass flow meter was installed in the liquid line, which could guarantee it measures subcooled liquid all the time and acquire more accurate and stable reading.

3.5.4 AC Watt Transducer

Ohio Semitronics GH020D was installed to measure the power consumption of the outdoor unit, which consists of fan power and compressor power as shown in Figure 11. Both the fan and compressor have only single-speed operation and fan power would reach at steady state in a very short time compared to the response time of compressor during start-up. Thus, the transient profile of total power consumption shares the same trend as the profile of the compressor. Moreover, in real-life unit, each single outdoor unit incorporates a fan with the heat exchanger coils, and the total power consumption of the outdoor unit was used to calculate the system COP. An electrical metallic

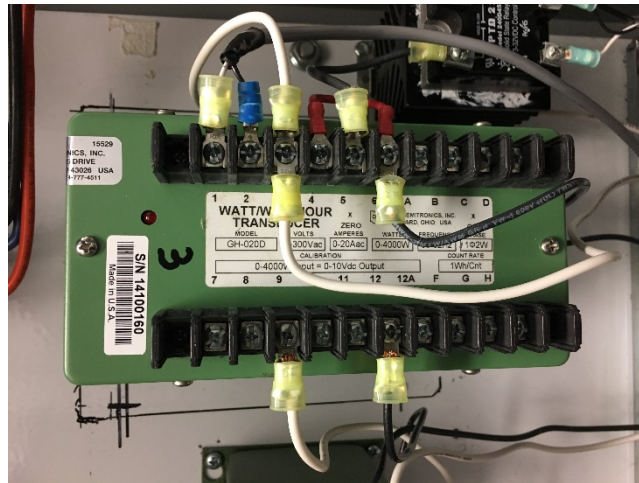


Figure 11: Ohio Semitronics AC Watt Transducer



Figure 12: Overview of the Electric Box and the Variac for Outdoor Unit Power Supply

enclosure was built for the power supply for the outdoor unit as shown in Figure 12.

Due to the under-voltage of our lab, an AC variac was installed to guarantee the compressor runs under rated power of 230V all the time as shown in Figure 12.

3.5.5 Dewpoint Sensor

Two EdgeTech DewTrak II dewpoint sensors as shown in Figure 13 were installed at the inlet and outlet of the indoor unit to measure the dewpoint of air blowing through the unit. The dewpoint data was used to calculate the latent cooling capacity under wet-coil testing conditions (ASHRAE A and B). Moreover, the latent cooling capacity was also calculated based on the flow rate of condensate from the indoor unit, and the comparison of results is discussed in the following chapter. The dewpoint sensor can measure the humidity more accurately than a relative humidity sensor at the cost of its response time.

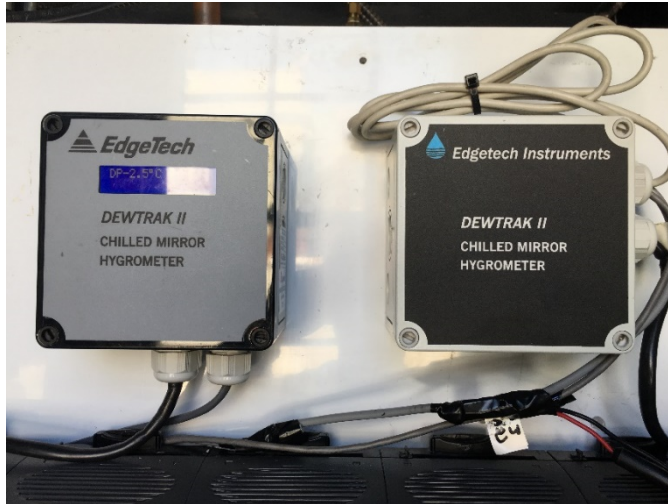


Figure 13: DewTrak II Dewpoint Sensor

3.5.6 Air Damper

Johnson Control customized air dampers with electrical dampers as shown in Figure 14 were installed at the inlet and outlet of the testing and bypass duct respectively. The



Figure 14: Air Damper with Electrical Actuator

dampers can be actuated with a LabVIEW program, which is convenient to control during the cyclic test. However, the electrical actuator on the damper usually has a long response time. For our dampers, the opening time is 60 seconds while 20 seconds of closing. Considering the ON period of cyclic testing is only 6 minutes, the two dampers on the testing duct are switched manually in the following tests.

3.5.7 Quick Closing Valve

To isolate the AC unit into several sections, three Assured-Automation Coaxial valves as shown in Figure 15 were installed at the condenser outlet, TXV inlet and compressor suction. By actuating those valves at the same time as shutting off the compressor, the refrigerant loop is separated into three sections, namely, outdoor unit section, liquid line section, and indoor unit plus vapor line section as shown in Figure 3. Due to the unidirectional differential pressure rating of 4,137 kPa, after isolating the system, a



Figure 15: Assured-Automation Quick Closing Valve

certain order to open the releasing ball valves to ensure the differential pressure across the valve is within the allowed range. In addition, the valve generates heat when it is operated, which will heat up the refrigerant in the sections of piping close to those valves. To minimize the effect of the heat on the vapor refrigerant density, a portable fan was set up to cool down the adjacent space of those valves as much as possible.

3.5.8 Recovery Compressor

In the charge distribution tests, after expanding all the refrigerant to expansion tanks, a recovery compressor was installed in the returning piping from the expansion tanks back to system. The suction piping was connected to the six expansion tanks and discharge was connected to the liquid line, and on both sides ball valves were installed to isolate the compressor when the system was in normal operation and expansion period. And an electrical box was built to control the recovery compressor as shown in Figure 16.



Figure 16: Electrical Box to Control the Recovery Compressor

A starting capacitor was properly sized and installed to start up the compressor, a solid-state relay was installed and in serial to incorporate the control signal from the data acquisition system, by which the compressor can be turn on and off by clicking on one bottom in the LabVIEW program.

Ideally, all the refrigerants expanded to the expansion tanks should be recovered to the test unit maintain the same system performance. However, considering the mechanism of the compressor, it cannot evacuate the system in a deep vacuum pressure, too large pressure ratio of discharge to suction could damage the compressor. And it would increase the power consumption and raise the discharge temperature a lot, which is also detrimental to the compressor. Therefore, the test compressor was stopped after each test while the recovery compressor pulls down to the vacuum pressure in expansion tanks and the residual amount of refrigerant left in the expansion system was calculated based on the density. That residual amount was subtracted from the total charged amount to obtain the amount of charge recovered. In addition, a charge sensitivity test which is discussed in the following chapter was conducted to guarantee the same system remains the same performance after every expansion process.

3.5.9 Summary

The information about the chosen instruments and descriptions on installation and operation have been provided in the above sections. The range and accuracy specifications are summarized in Table 2.

Table 2: Specification of Installed Instrumentations

	Manufacturer	Range	Accuracy
Air Differential Pressure	SETRA Model 264	0 – 0.622 kPa 0 – 1.245 kPa	±0.4 %F.S. ±1.0 %F.S.
Barometric Pressure	SETRA Model 278	600 – 1100 mbar	±0.3 mbar
Ref. Absolute Pressure	SETRA Model 280	0 – 3447 kPa	±0.11 %F.S.
Ref. Differential Pressure	OMEGA PX419	0 – 34.47 kPa	±0.08 %
	SETRA Model 230	0 – 34.47 kPa	±0.25 %F.S.
Thermocouple	OMEGA T Type	-270 – 400°C	±0.5°C
Mass Flow Meter	Emerson Micromotion 2700	0 – 50 g/s	±0.2%
AC Watt Transducer	Ohio Semitronics GH020D	0 – 4 kW	±0.2 %
Dewpoint Sensor	EdgeTech DewTrak II	-40 – 60 °C	±0.2°C

3.6 Data Acquisition System

All the instrumentations which output an electric signal, either current or voltage, were wired to NI data acquisition (DAQ) modules as shown in Figure 17 and Figure 18. Two



Figure 17: NI Data Acquisition Modules of the Code Tester

sets of DAQ modules were set up for the code tester and the psychrometric chamber, respectively.

Different modules were designed for different instrumentations including analog input, thermocouple, digital output and analog output modules. Different channel configurations on the analog input module were chosen depending on the types of output signals of different type of transducers. And analog output modules were used to send out control signal from the DAQ to instrumentations including air damper and quick closing valve. With a data recording program coded by LabVIEW, all the test data was recorded and saved to Excel file automatically. And the scan rate of data recording was set to be 1 second during the test. In addition, LabVIEW program was coded to monitor the system parameters in a single window on a system diagram as shown in Figure 19.



Figure 18: NI Data Acquisition Modules of the Outdoor Unit

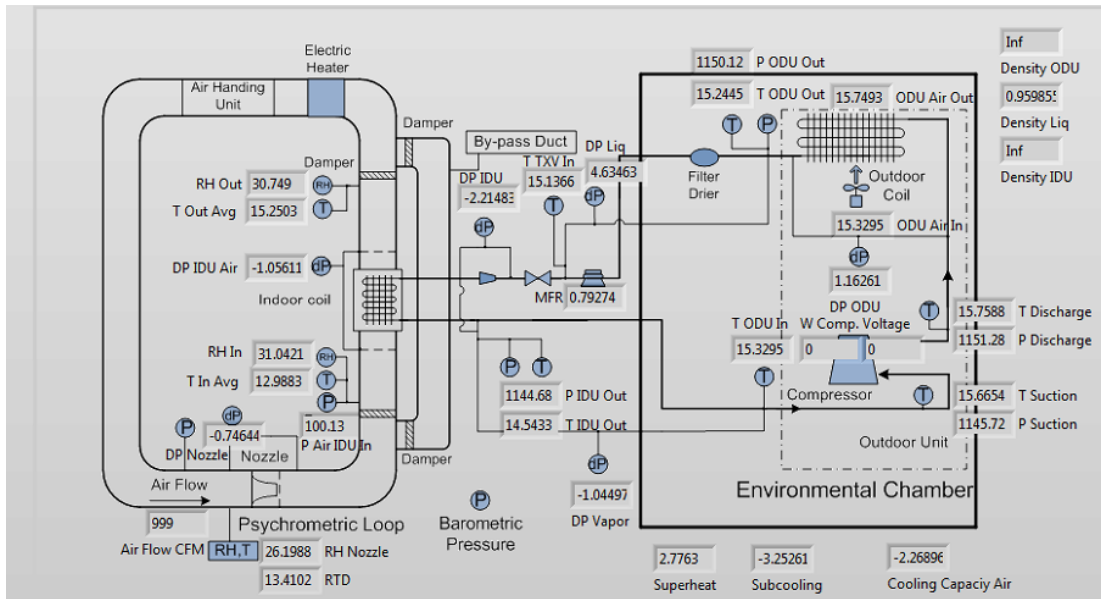


Figure 19: Data Visualization Window in LabVIEW Program

As shown in Figure 19, calculated parameters such as air-side cooling capacity can also be displayed with those direct-measured parameters, which is of importance for monitoring the system when it is in ON period and have the sense whether the system behaves well or not.

3.7 Uncertainty Analysis

Uncertainty analysis is of importance together with mean value to represent the accuracy and reliability of the test data obtained. The total uncertainty comes from two major sources, one is called systematic uncertainty which is mostly caused by instrumentation itself and can be specified by the manufacturer, and another is called random uncertainty which describes the range of measured data and can be estimated by standard deviation calculation as shown in Eq. (1).

$$\varepsilon_{STD} = \sqrt{\frac{1}{N-1} \sum_{i=1}^N (x_i - \bar{x})^2} \quad (1)$$

Where:

N = number of scans of data in a sample

x_i = data at point of index i

\bar{x} = mean value of all data in a sample

Total uncertainty of direct-measured parameters can be calculated as Eq. (2).

$$\varepsilon_{total} = \sqrt{\varepsilon_{sys}^2 + \varepsilon_{STD}^2} \quad (2)$$

Where:

ε_{total} = total uncertainty

ε_{sys} = systematic uncertainty

ε_{STD} = random uncertainty estimated by standard deviation

At this test facility, direct-measured variables include temperature, dewpoint temperature, pressure, refrigerant mass flow rate, and power consumption. And calculated parameters based on those direct-measured variables include superheat, subcooling, enthalpy, airflow rate, cooling capacity, and COP.

Total uncertainty of calculated parameters can be computed as Eq. (3).

$$\varepsilon_{total,f} = \sqrt{\left(\frac{\partial f}{\partial x_1} \varepsilon_{x_1}\right)^2 + \left(\frac{\partial f}{\partial x_2} \varepsilon_{x_2}\right)^2 + \dots + \left(\frac{\partial f}{\partial x_i} \varepsilon_{x_i}\right)^2 + \dots} \quad (3)$$

Where:

f = calculate parameter based on direct-measured variables $x_1 \dots x_n$

ε_{x_i} = total uncertainty of direct-measured variables of index i

The systematic uncertainties of direct-measured variables are summarized in Table 3.

Table 3: Systematic Uncertainties of Direct-measured Variables

Variables*	Value	Sys. Uncertainty
Cond. Outlet Pressure (kPa)	2734.3	3.8
TXV Outlet Pressure (kPa)	1304.6	3.8
Evap. Outlet Pressure (kPa)	1094.5	3.8
Cond. dP (kPa)	56.4	0.2
Liquid Line dP (kPa)	25.434	0.345
Vapor Line dP (kPa)	4.923	0.004
Cond. Outlet Temp. (°C)	37.5	0.5
TXV Inlet Temp. (°C)	35.4	0.5
Evap. Outlet Temp. (°C)	14.0	0.5
Compressor Suction Temp. (°C)	20.4	0.5
Refrigerant Mass Flow Rate (g/s)	32.0	0.1
ODU Power Consumption (W)	1263.8	2.5

* Comp., Cond., Evap., dP, temp., and ODU stand for compressor, condenser, evaporator, differential pressure, temperature, outdoor unit, respectively. And all the data are obtained under ASHRAE A condition.

Chapter 4 : Test Results and Data Analysis

4.1 Steady-state Condition Baseline Test

4.1.1 Charge Calibration

A charge calibration test was conducted. The goal is to match the system superheat and subcooling under ASHRAE A, B, and C conditions to those tested in manufacturer's lab under the same steady-state condition. Since the liquid line in the test facility at University of Maryland, College Park (UMCP) was 3 meters longer than that of the test facility at manufacturer's laboratory, more system charge was expected for our test facility. As shown in Table 4, the system charge at UMCP was adjusted according to data provided by the manufacturer in terms of condenser outlet subcooling.

Table 4: Charge Calibration under Steady-state Conditions

		Manufacturer	UMCP
Total System Charge (kg)		2.22	2.40
ASHRAE A	Subcooling (K)	7.8	7.5
	Superheat (K)	2.6	3.7
ASHRAE B	Subcooling (K)	5.6	5.6
	Superheat (K)	2.9	3.8
ASHRAE C	Subcooling (K)	6.2	6.0
	Superheat (K)	2.7	4.7

Since the TXV originally equipped with the unit was replaced due to the hunting issue, the system superheat values were 1-2 degree Celsius higher than those of

manufacturer’s data. With respect to the total system charge, the extra 180 g of R410A charge is mainly caused by the extra length of the refrigerant piping at UMCP compared to those at manufacturer’s lab. And the validation of extra charge of 180 g R410A is presented in Table 5.

Table 5: Validation of Extra System Charge

	Liquid Line	Vapor Line
Extra length (m)	3.05	3.05
OD (mm)	9.5	19.1
Volume (cm ³)	148.4	652.5
Density (kg/m ³) *	997.7	41.1
Mass (kg)	0.15	0.03
Total Extra Charge (kg)	0.18	

*Properties of refrigerant are calculated based on the data under ASHRAE A steady-state condition

4.1.2 Data Summary (ASHRAE A, B, and C Tests)

Steady-state baseline tests were carried out under conditions presented in Table 1. All the data summarized in this chapter were recorded for 30 minutes after all the system parameters reach in steady state. Usually it took 1-2 hours for the unit to reach steady state. Table 6, Table 7, and Table 8 are the data summary under ASHRAE A, B, and C conditions respectively.

Table 6: Data Summary of ASHRAE A Condition Test

Parameter	Value	Systematic Uncertainty	Random Uncertainty	Total Uncertainty
P Cond. Outlet (kPa)	2,734.3	3.8	4.9	6.2
P Evap. Outlet (kPa)	1,094.5	3.8	0.9	3.9
T Cond. Outlet (°C)	37.5	0.5	0.1	0.5
T Evap. Outlet (°C)	14.0	0.5	0.2	0.5
T Air Evap. Inlet (°C)	26.1	0.5	0.0	0.5
T Air Evap. Outlet (°C)	13.9	0.5	0.0	0.5
Ref. Mass Flow Rate (g/s)	32.0	0.1	0.1	0.1
Outdoor Power Consumption (kW)	1.263	0.003	0.002	0.004
Cooling Capacity (Air) (kW)	5.20	-	-	0.24
Cooling Capacity (Ref.) (kW)	5.26	-	-	0.04
Energy Balance (%)	1.01	-	-	0.05
COP	3.53	-	-	0.16

Table 7: Data Summary of ASHRAE B Condition Test

Parameter	Value	Systematic Uncertainty	Radom Uncertainty	Total Uncertainty
P Cond. Outlet (kPa)	2,250.3	3.8	2.9	4.8
P Evap. Outlet (kPa)	1,076.8	3.8	2.1	4.3
T Cond. Outlet (°C)	31.3	0.5	0.1	0.5
T Evap. Outlet (°C)	13.5	0.5	0.2	0.5
T Air Evap. Inlet (°C)	26.0	0.5	0.0	0.5
T Air Evap. Outlet (°C)	13.4	0.5	0.1	0.5
Ref. Mass Flow Rate (g/s)	32.1	0.1	0.1	0.1
Outdoor Power Consumption (kW)	1.049	0.002	0.002	0.003
Cooling Capacity (Air) (kW)	5.43	-	-	0.24
Cooling Capacity (Ref.) (kW)	5.58	-	-	0.04
Energy Balance (%)	2.47	-	-	0.05
COP	4.34	-	-	0.19

Table 8: Data Summary of ASHRAE C Condition Test

Parameter	Value	Systematic Uncertainty	Random Uncertainty	Total Uncertainty
P Cond. Outlet (kPa)	2,218.0	3.8	3.8	5.3
P Evap. Outlet (kPa)	991.6	3.8	1.0	3.9
T Cond. Outlet (°C)	30.4	0.5	0.1	0.5
T Evap. Outlet (°C)	11.5	0.5	0.2	0.6
T Air Evap. Inlet (°C)	26.7	0.5	0.0	0.5
T Air Evap. Outlet (°C)	11.0	0.5	0.0	0.5
Ref. Mass Flow Rate (g/s)	29.2	0.1	0.1	0.2
Outdoor Power Consumption (kW)	1.050	0.002	0.002	0.003
Cooling Capacity (Air) (kW)	5.09	-	-	0.24
Cooling Capacity (Ref.) (kW)	5.09	-	-	0.04
Energy Balance (%)	0.03	-	-	0.05
COP	4.01	-	-	0.19

* P, T, Cond., Evap., Ref., stand for pressure, temperature, condenser, evaporator, and refrigerant, respectively.

The air-side cooling capacity is calculated as Eq. (4).

$$\dot{Q}_{air} = \dot{Q}_{sen} + \dot{Q}_{lat} \quad (4)$$

Where:

\dot{Q}_{air} = total air-side cooling capacity

\dot{Q}_{sen} = air-side sensible cooling capacity

\dot{Q}_{lat} = air-side latent cooling capacity

Sensible cooling capacity is calculated as Eq. (5).

$$\dot{Q}_{sen} = \frac{\dot{Q}_{mi} \bar{c}_p (t_{a1} - t_{a2})}{v_n} \quad (5)$$

Where:

\dot{Q}_{mi} = measured indoor airflow

\bar{c}_p = average specific heat of air blowing through IDU

t_{a1} = temperature of the air entering IDU

t_{a2} = temperature of the air leaving IDU

v_n = specific volume of dry air entering IDU

Latent cooling capacity is calculated as Eq.(6). And latent cooling capacity is zero under dry-coil test conditions.

$$\dot{Q}_{lat} = 2.47 \times 10^6 \frac{\dot{Q}_{mi} (W_1 - W_2)}{v_n} \quad (6)$$

Where:

W_1 = humidity ratio of air entering IDU

W_2 = humidity ratio of air leaving IDU

It should be noted that the latent cooling capacity is a function of the latent heat of vaporization h_{fg} of water, in Eq. (6), the h_{fg} at 13°C is used ($h_{fg} = 2.47 \times 10^6 \text{ J/kg}$) and the energy associated with the leaving condensate was neglected due to its small flow rate and its negligible impact on cooling capacity.

Refrigerant-side cooling capacity is calculated as Eq. (7).

$$\dot{Q}_{ref} = \dot{m}_{ref} (h_{r2} - h_{r1}) \quad (7)$$

Where:

\dot{Q}_{ref} = refrigerant-side cooling capacity

h_{r1} = enthalpy of refrigerant entering evaporator

h_{r2} = enthalpy of refrigerant leaving evaporator

Energy balance (EB) is calculated as Eq. (8).

$$EB = \frac{(\dot{Q}_{ref} - \dot{Q}_{air})}{\dot{Q}_{ref}} \times 100\% \quad (8)$$

Coefficient of performance (COP) is calculated as Eq. (9).

$$COP = \frac{(\dot{Q}_{ref} + \dot{Q}_{air})/2 - P_{df}}{P_{ODU} + P_{df}} \quad (9)$$

Where:

P_{df} = default fan power of commercial indoor units

P_{ODU} = ODU power consumption

The cooling capacity data presented in Table 6, Table 7, and Table 8 are calculated values from measured variables after subtracting the default fan power for indoor unit, because the indoor unit tested in the code tester doesn't have a fan, while the commercial unit has a fan on top the coil. Thus, to evaluate the COP as an indicator of the system performance of a commercial unit, we need to subtract that default fan power from the cooling capacity measured. And the total power consumption in the denominator of COP consists of outdoor unit power consumption and the default fan power.

As shown in Table 6, Table 7, and Table 8, the unit has highest cooling capacity and COP under ASHRAE B condition, which is a wet-coil and mild-outdoor-temperature condition. On the contrary, the unit has the lowest system performance under ASHRAE

A condition, which is a wet-coil and high-outdoor-temperature condition. The calculated total uncertainty of air-side cooling capacity is considerably larger than that of refrigerant-side, which is mainly caused by the uncertainty of air temperature measurement of 0.5°C.

As for repeatability, the baseline tests were repeated in three times first and in multiple times after modifications made on the test facility. The system demonstrated good repeatability of steady-state performance in 3%.

4.2 Cyclic Condition Test

4.2.1 Data Summary (ASHRAE D Test)

The setting temperature and relative humidity of ASHRAE D condition are the same as those of ASHRAE C condition. And the cyclic operation of unit starts after at least two-hour steady state under ASHRAE C condition, which could guarantee all the system parameters reach in steady state, especially coil temperatures. A 24-minute OFF period followed by a 6-minute ON period is regarded as a complete cycle of the cyclic test, and it is repeated consecutively for three times to be recorded as one set of cyclic test data (90 min).

The system parameters with respect to time are shown in the following figures. Figure 20 presents the refrigerant temperature along the refrigerant loop changes with time during the cyclic operation. The compressor discharge temperature has a distinct peak at the beginning of start-up and gradually increases from 40°C to 57°C in 6 min. The condenser outlet temperature is relatively high in the first 3 min of start-up, so that the

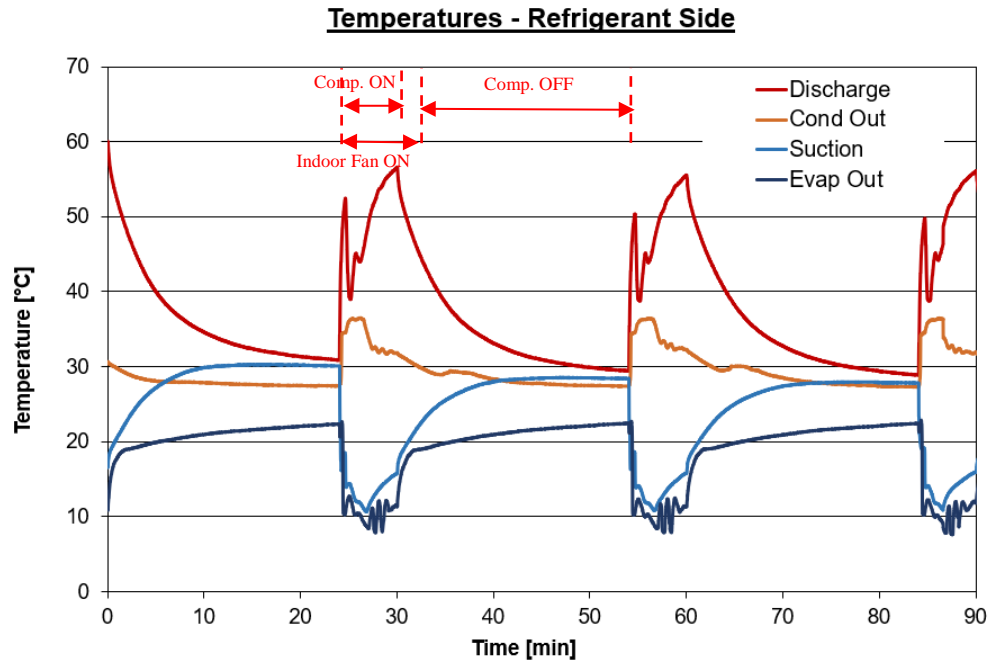


Figure 20: Refrigerant Temperature versus Time under Cyclic Condition

system subcooling is low. The reason for the slow response of subcooling is mostly is that the refrigerant mass is building up at first 2 min and the condenser and evaporator coils needs time to overcome its thermal inertia. The compressor suction temperature drops quickly in the first 2 min of start-up and gradually increases as the increase of evaporator outlet temperature. And the evaporator temperature shows a similar but more smooth behavior as the suction temperature and we need to note that in the last 3 min of start-up, the evaporator outlet is starting to oscillate, which is the characteristic of TXV control on superheat. As for shut-down period, the compressor discharge and suction temperature present a relative smooth equalization with ambient while the evaporator outlet shows a rapid heat exchange with ambient due to a delay time of fan keeping blowing air through the indoor unit coil. And the condenser outlet temperature

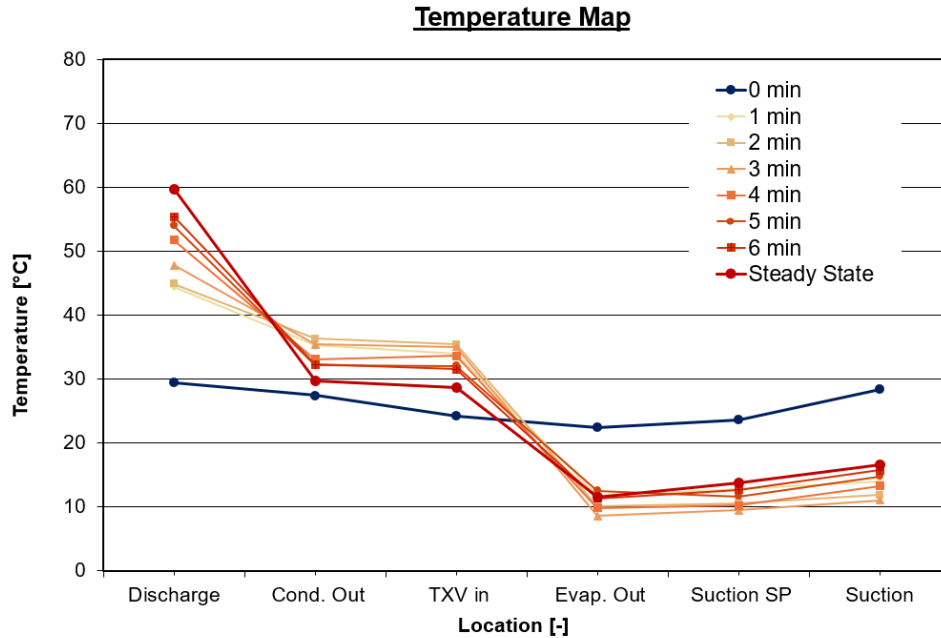


Figure 21: Refrigerant Temperature Map during Start-up

presents the least change during the shut-down period as its temperature is close to the chamber ambient temperature at the end of the start-up period.

Figure 21 presents the refrigerant temperature at six locations along the refrigerant loop varies every one minute during ON period. The high-temperature side increases and reaches its 6-min values slower than the low-temperature side. And the same conclusion can be drawn from above two figures that the evaporator outlet temperature has the fastest response, while the response of compressor discharge temperature is the slowest. In addition, the refrigerant temperatures do not fully equalize at the end of shut-down period which is as shown in the dark blue line in the figure, but it generally demonstrated a similar trend as the 6-min temperature profile.

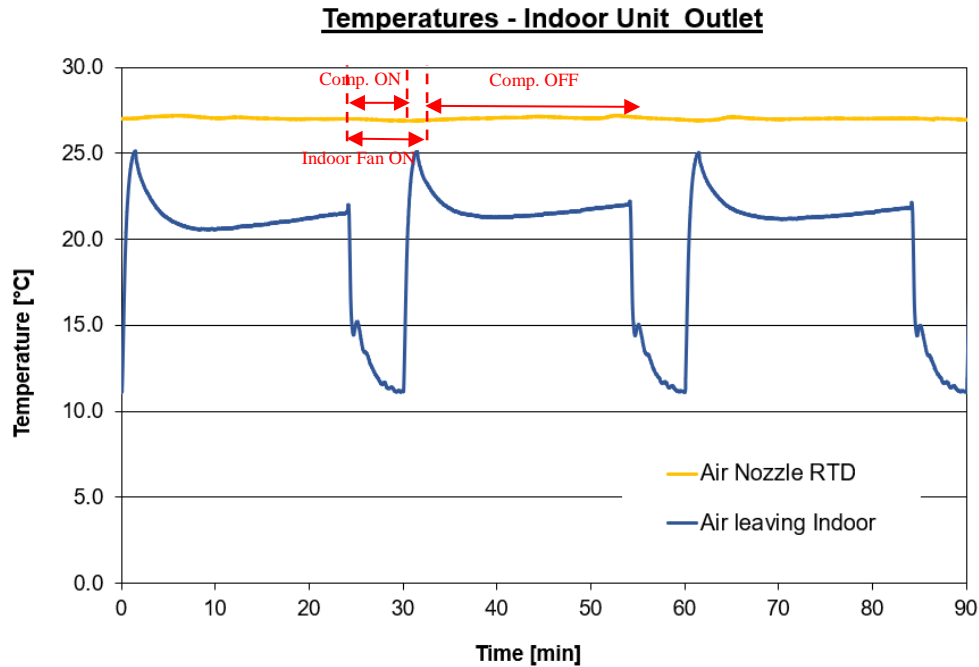


Figure 22: Air Entering and Leaving Temperature of Indoor Unit under Cyclic Condition

Figure 22 shows the entering and leaving air temperature of indoor unit vary under cyclic operation. Entering air was controlled by the air handling unit in the code tester, so it is 26.7°C throughout the cyclic test. As for the leaving air temperature, it drastically drops from 22°C to 15°C as the compressor starts and then gradually decrease to 11°C, which is close to the steady-state value under ASHRAE C condition. As compressor shuts down and airflow keeps blowing the indoor unit for another 1.5 min (fan delay period), the leaving temperature is 25°C at the end of 7.5 min airflow blowing time since the external surface of the evaporator coil is still at low temperature even if the compressor shuts down. After 7.5 min, the airflow is directed to bypass duct by the air dampers. However, the air leaving the indoor unit keeps dropping during the shut-down period, which is due to the thermal mass of the code tester. Specifically, the

duct pieces and mixer are cooled down during start-up period and they cool down the air in the testing duct during shut-down period. Moreover, the design of the code tester decides how much thermal inertia it has, which has a direct impact on the cooling capacity stored in the duct components during start-up period. Therefore, different degrees of cyclic degradation are expected if the air-conditioning unit is tested in different code tester. And this is discussed more in detail in the following sections.

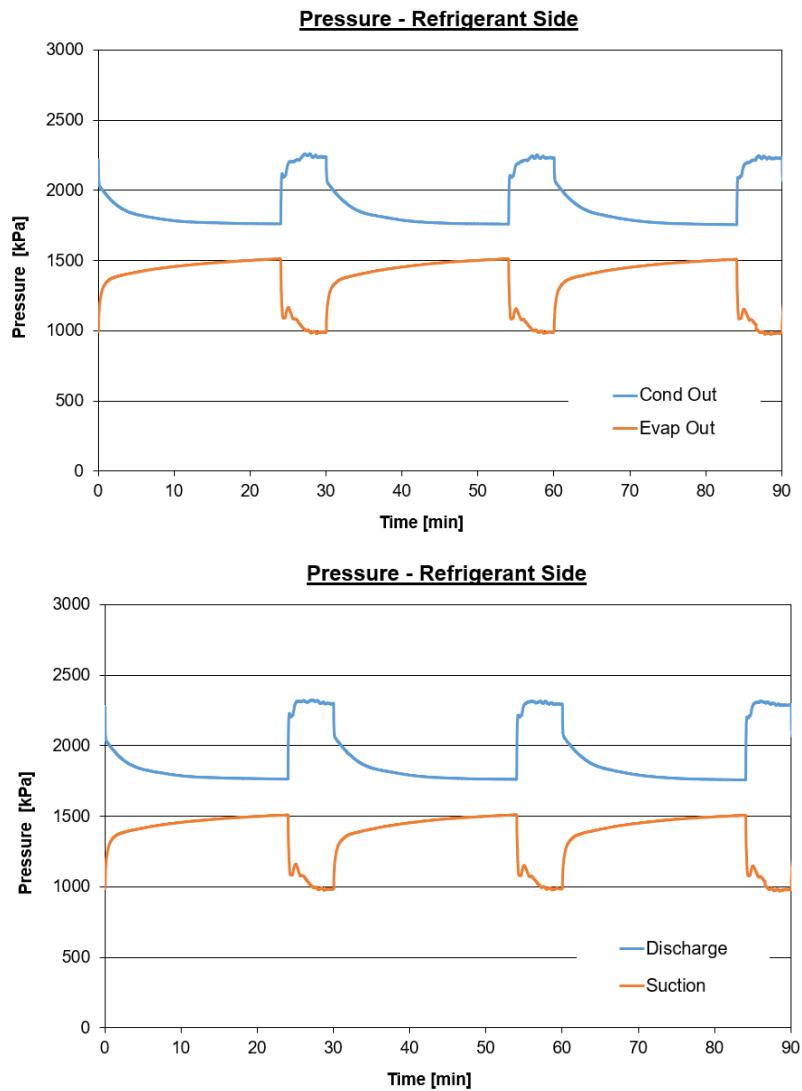


Figure 23: Refrigerant Pressure under Cyclic Condition

Figure 23 presents the refrigerant pressure variation with time during cyclic condition. The pressures response much faster than temperatures, and high-side pressure builds up faster than low-side pressure during start-up period. And during the shut-down period, both high-side pressure and low-side pressure drop rapidly at the time when compressor shuts down, and then gradually reach a differential pressure of 500 kPa. As the TXV and compressor both are designed to have leak-proof mechanisms between two pressure sides, the system pressure doesn't equalize during the shut-down period, which means there could be less refrigerant migrating from high side to low side during the shut-down period than the system without those leak-proof mechanisms. And it is of importance to have lower thermal inertia in next start-up so as to have better system cyclic performance.

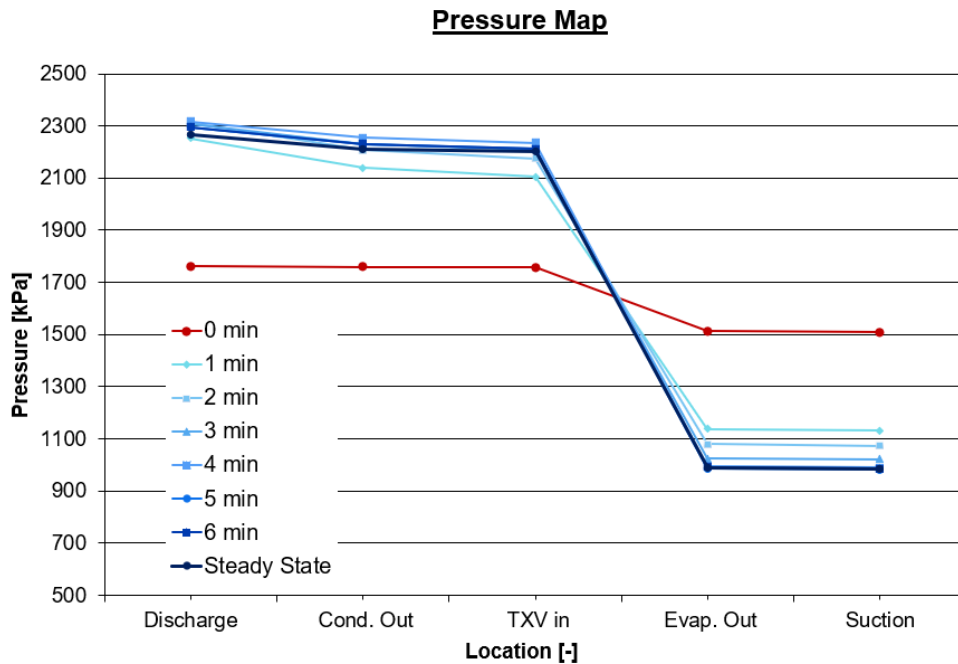


Figure 24: Refrigerant Pressure Map during Start-up

Figure 24 shows refrigerant pressure behaviors along the refrigerant loop during 6 min ON period. As observed, the compressor discharge pressure gets close to its 6-min value in the shortest time, while the other four pressures behave similarly in terms of response speed. As mentioned above, due to the anti-leak technical designs of TXV and compressor, there is a distinct differential pressure between high-side and low-side pressure at the end of the shut-down period.

Figure 25 presents the refrigerant differential pressure across the condenser coil, liquid line, evaporator coil and liquid line, which would be valuable data for the future validation of transient model of air-conditioning unit. At the beginning of start-up period, the refrigerant mass flow rate increases sharply and has a peak, as a result, the differential pressures along the refrigerant loop also reach the maximum values. And in the first 3 min of the start-up period, the differential pressures gradually decrease

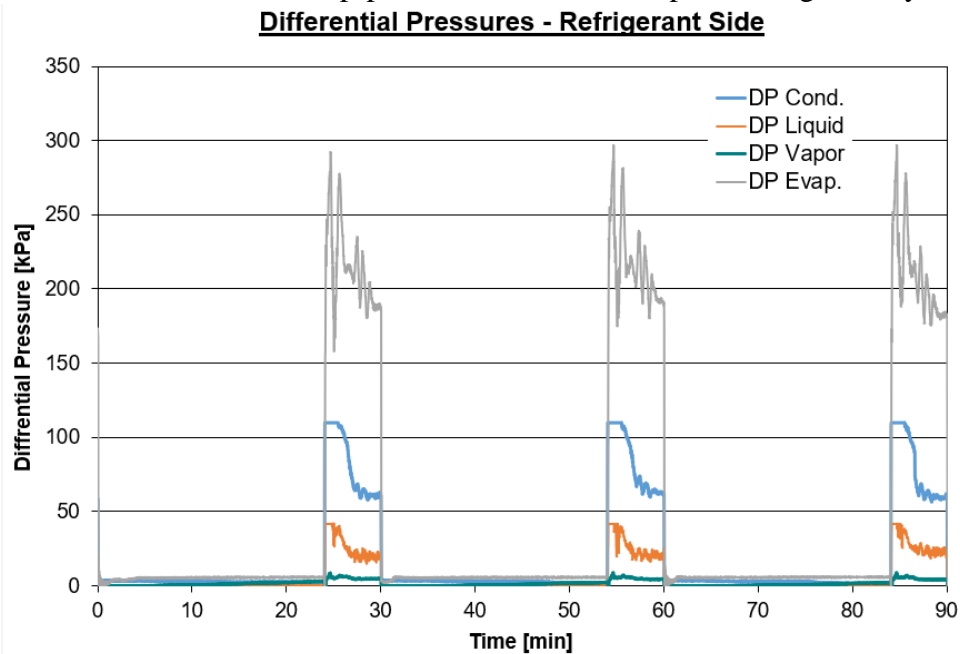


Figure 25: Refrigerant Differential Pressure across Components during Cyclic Condition

and reach cyclic stable values, which have the similar trend as the refrigerant mass flow rate. In addition, the differential pressure across the evaporator coil consists of the differential pressure across the distributor, feeder tubes and the coils. Thus, the cyclic stable value is over 150 kPa, which is two times as the common pressure drop designed for a single evaporator coil.

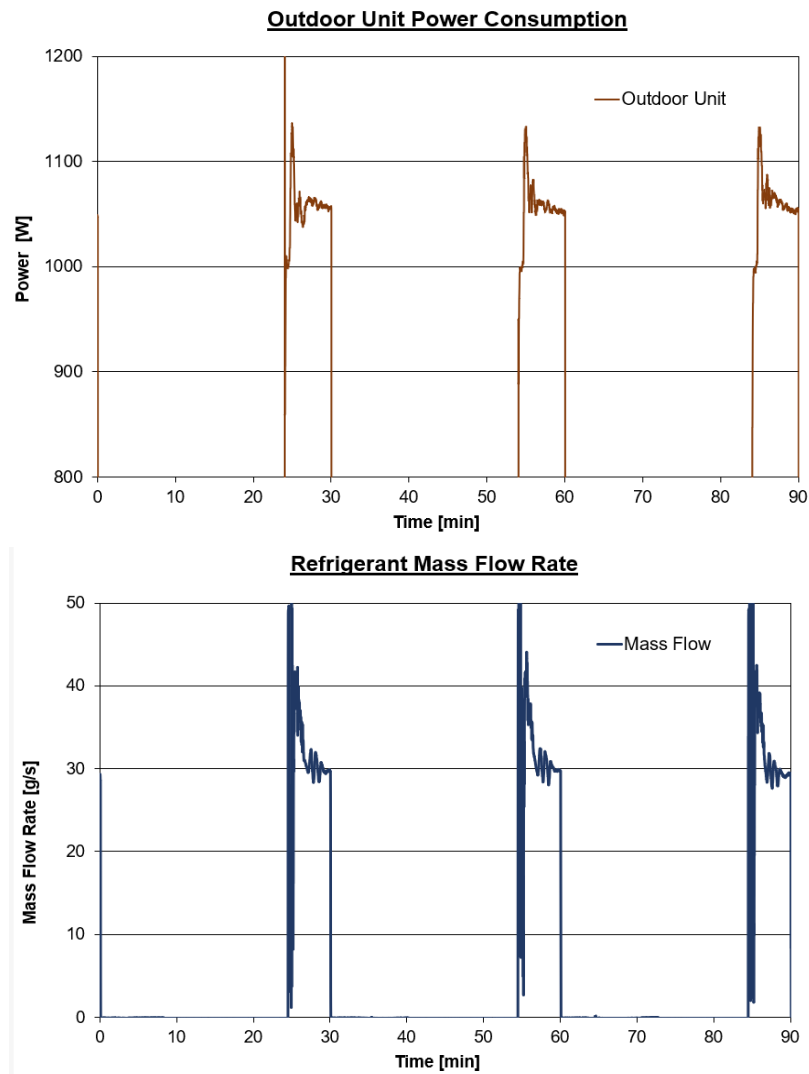


Figure 26: Outdoor Unit Power Consumption and Refrigerant Mass Flow Rate during Cyclic Condition

Figure 26 provides the transient behavior of outdoor unit power consumption and refrigerant mass flow during the cyclic condition. In general, these two have similar transient response, because they are essentially related to each other. As the compressor starts, the initial torque to overcome all the static frictions of the fan motor and compressor motor draws a huge starting current, thus the power consumption of the unit has a peak at the beginning of the start-up period. And then the power consumption reaches its cyclic steady-state value in 3 min or so. The refrigerant mass flow rate basically behaves similarly as the power consumption, but relatively delayed response and it takes longer for it reaching cyclic stable value compared to the outdoor unit power consumption.

Figure 27 presents the refrigerant-side and air-side cooling capacity calculated based on the measured variables. Overall, the response of refrigerant-side cooling capacity is

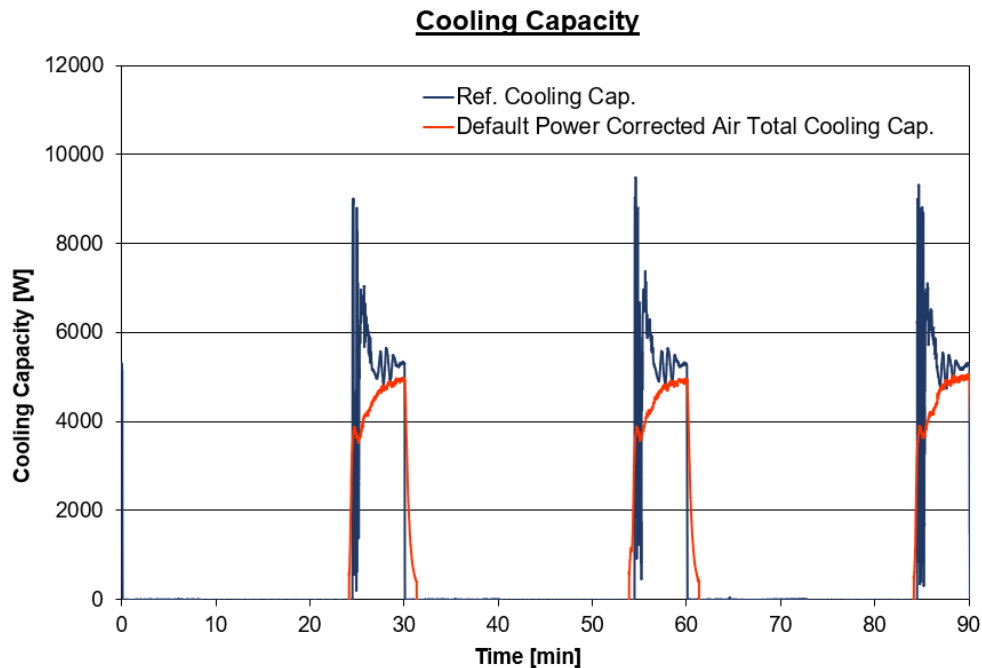


Figure 27: Cooling Capacity during Cyclic Condition

faster than that of air-side. The reason for the slower response of air-side cooling capacity is that the capacity is calculated based on the difference of entering and leaving air stream of indoor unit, it takes some time for the heat exchange between the refrigerant inside the evaporator tubes and the circulating air in the code tester. It should be noted that there is a 1.5 min fan delay time after the 6 min ON time, in which the air keeps blowing through the indoor unit. Therefore, there is also an extra portion cooling capacity captured due to the low temperature of the evaporator coil surface. In addition, the cyclic stable value of refrigerant-side cooling capacity is 300 W higher than that of air-side. This phenomenon can also be justified with the thermal mass impact as follows. During the shut-down period, the testing duct keeps cooling down the air and increases to a relatively high temperature so that it could store a certain portion of cooling capacity during the following start-up period. Thus, that difference between refrigerant-side and air-side can be validated with the thermal mass of the code tester and this aspect is discussed in the later section.

4.2.2 Evaluation of the Degradation Coefficient

To evaluate the efficiency loss due to the cyclic operation of the unit, the degradation coefficient (C_d) is calculated based on the data under ASHRAE C and D conditions.

The C_d is defined as Eq. (10).

$$C_d = \frac{(1 - \frac{EER_{cyc}}{EER_{ss}})}{(1 - CLF)} \quad (10)$$

Where:

EER_{cyc} = energy efficient ratio under cyclic condition

EER_{ss} = energy efficient ratio under steady-state condition

CLF = cooling load factor

The steady-state and cyclic EER are determined by Eq. (11) and Eq. (12), respectively.

$$EER_{ss} = \dot{q}_{tci} / \dot{E}_t \quad (11)$$

Where:

\dot{q}_{tci} = indoor air-side total cooling capacity (Btu/h)

\dot{E}_t = total power input (W)

$$EER_{cyc} = q_{cyc} / E_{cyc} \quad (12)$$

Where:

q_{cyc} = indoor air-side total integrated capacity during cyclic operation (Btu)

E_{cyc} = total power input during cyclic operation consisting of one compressor ON and one compressor OFF period (W*h)

In this study, the calculated cooling capacity and measured power consumption were recorded every one second and integrated in a spreadsheet by adding data at all points, multiplying by sampling time interval, and divided by the total sampling time. In addition, all those integrations mentioned were done using the data of the second ON period of the cyclic test.

The cooling load factor is determined as Eq. (13).

$$CLF = q_{cyc} / (\dot{q}_{tci} \cdot t_{cyc}) \quad (13)$$

Where:

t_{cyc} = duration of time for one complete cycle consisting of one compressor ON time and one compressor OFF time (hours)

With the nature of definition of the degradation coefficient, it could have a much larger uncertainty relative to its measured mean value. To demonstrate the repeatability of the test data, five repeated tests under ASHRAE D condition were conducted and C_d is calculated for each test and the test results are shown in Table 9.

Table 9: Evaluation of Degradation Coefficient of Five Cyclic Tests

	Test 1	Test 2	Test 3	Test 4	Test 5
EER_{cyc}	11.986	12.128	12.008	11.913	11.809
EER_{ss}	13.531	13.616	13.338	13.338	13.333
CLF	0.183	0.182	0.186	0.185	0.183
C_d	0.140	0.134	0.123	0.131	0.140
$C_{d_Avg.}$			0.134		
Std. Dev.			0.007		
Rel. Std. Dev.			0.052		

* Avg., Std. Dev., and Rel. Std. Dev. stand for average, standard deviation, and relative standard deviation.

As shown in the above table, five repeated cyclic tests have an average C_d calculated to be 0.134 and the relative value of standard deviation is 5.2%, which is acceptable considering the large-uncertainty nature of the C_d . Therefore, the average value of C_d measured at UMCP is reliable enough to represent the coefficient loss of the unit tested during cyclic condition operation. As compared to the default value of 0.25 [32] is used

to evaluate the system performance under ASHRAE C and D condition, the C_d calculated in this study is only 0.13. Obviously, the unit cyclic performance could be under-predicted if that default value is used in performance estimation. Moreover, the design of the code tester used to test the unit can have an impact on the calculated C_d , so that different C_d values are expected from data of different code tester. Therefore, one important goal of future study is to normalize the effects of code tester on the evaluation of C_d , so that, the same cyclic performance would be reported even if the same unit is tested in two totally different test facilities.

4.2.3 Effect of Thermal Mass of the Code Tester

As mentioned in the previous sections, the thermal mass of code tester has an impact on transient cooling capacity during the cyclic test, the cooling capacity of the second ON period are compared in Figure 28. The yellow solid line is the cooling capacity at UMCP and blue dashed line is the cooling capacity from manufacturer's testing data

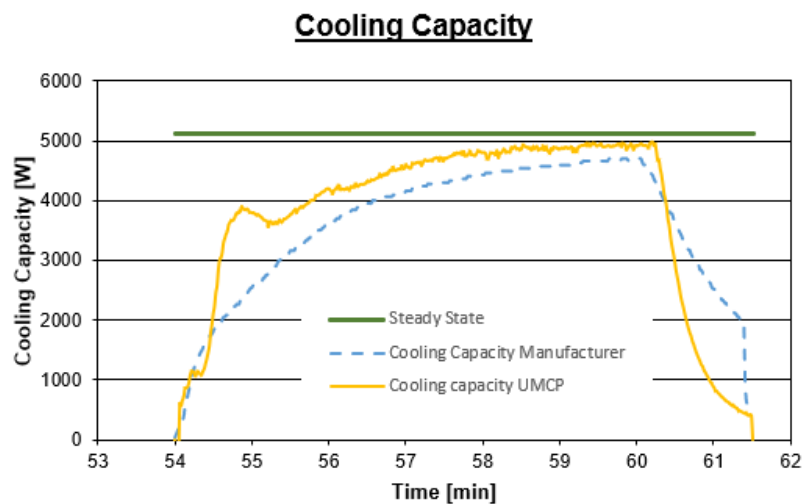


Figure 28: Cooling Capacity Comparison under the Cyclic Condition

of the same unit. And the green solid is the steady-state cooling capacity under ASHRAE C condition. The compressor is on from 54 min to 60 min and there is a 1.5-min fan delay time during which the air keeps blowing through the indoor unit. Since the dampers are switched at 54 min without ramping up the code tester fan, the cooling capacity at UMCP increases more drastically in the first minute. The peak is in accordance with the drastic drop of air leaving temperature presented in Figure 22. And the cooling capacity gradually gets close to the steady-state value, but it cannot achieve the same capacity in 6-min ON period. Moreover, the difference between those two cooling capacity profiles can be justified by the thermal mass of the code tester. The thermal mass of the UMCP code tester is much less than that of the manufacturer's, so much less cooling capacity is stored in the code tester during ON period, which results in lower air leaving temperature as well as higher capacity calculated. During 1.5-min fan delay period, the cold surface of evaporator coil and the code tester keep cooling down the blowing air. Less cooling capacity stored in the UMCP code tester results in less capacity released and higher leaving temperature, so that faster decrease of cooling capacity is observed from the UMCP data. Therefore, it is concluded that the thermal mass of the code tester does influence the performance evaluation of air-conditioning units and it is of importance that the variables in the code tester such as thermal mass need to be normalized in the unit evaluation process.

4.3 Refrigerant Charge Distribution Tests

In addition to evaluating the coefficient of C_d , refrigerant charge distribution under steady-state conditions is the first step to investigate the possibility of refrigerant charge reduction of the air-conditioning unit. Thus, refrigerant charge distribution test is proposed in this study to investigate how the system behaves during steady-state conditions in terms of refrigerant charge distribution among each system component, which is the basis of studying the charge migration under cyclic condition in the future study.

4.3.1 Internal Volume Calibration

Expansion method was implemented to measure the refrigerant charge of the system under steady-state condition. Basically, the mass of refrigerant is calculated with the density of vapor phase refrigerant and internal volume of each isolated system section. First of all, it is of importance to obtain the internal volume of each section and the accuracy of the internal volume value has a direct impact on the mass calculation later on. In this study, the R134a expansion method was proposed to measure the volume of each section. The reason was that R134a is a type of pure refrigerant so that it has more simple and accurate property functions than R410A REFPROP is used to calculate the properties of R134a and the uncertainty is typically 0.05% for density calculation [34]. The procedure of internal volume calibration test is as follows:

- 1) Evacuate the system and close the quick closing valve to isolate the system into three sections (outdoor unit section, liquid line section, indoor unit plus vapor line section)
- 2) Charge a sampling cylinder (5.9 L) with a certain amount of R134a weighted by the scale of mass m
- 3) Connect the sampling cylinder to test section and evacuate the piping in between
- 4) Open the releasing ball valve and vaporize all the R134a
- 5) Record the temperature and pressure data for 30 min after R134a reaching steady state and calculate its density ρ
- 6) Calculate the volume of section with density ρ and mass m
- 7) Repeat the same procedure for the other two sections

To eliminate the uncertainty of this method, four sets of tests are repeated for measuring the internal volume of each section and the results are presented in Table 10, Table 11, and Table 12.

Table 10: Internal Volume Measurement for Outdoor Unit Section

Parameter	Test 1	Test 2	Test 3	Test 4
Charged R134a (kg)	1.18	1.19	1.18	1.20
Pressure (kPa)	491.84	488.55	486.26	494.60
Temperature (°C)	23.3	19.8	18.9	19.4
Density (kg/m ³)	22.90	23.14	23.13	23.53
IV Measured (L)	51.35	51.42	51.20	51.08
IV Avg. (L)			51.26	
IV Std. Dev. (L)			0.15	
Rel. Std. Dev. (%)			0.29	

Table 11: Internal Volume Measurement for Indoor Unit plus Vapor Line Section

Parameter	Test 1	Test 2	Test 3	Test 4
Charged R134a (kg)	1.19	1.26	1.23	1.27
Pressure (kPa)	473.78	479.97	478.81	492.75
Temperature (°C)	22.1	19.0	19.5	19.8
Density (kg/m ³)	22.08	22.78	22.65	23.37
IV Measured (L)	53.80	55.31	54.32	54.52
IV Avg. (L)		54.49		
IV Std. Dev. (L)		0.63		
Rel. Std. Dev. (%)		1.15		

Table 12: Internal Volume Measurement for Liquid Line Section

Parameter	Test 1	Test 2	Test 3	Test 4
Charged R134a (kg)	1.33	1.09	1.26	1.23
Pressure (kPa)	548.44	452.99	519.15	507.73
Temperature (°C)	21.1	16.1	19.0	20.5
Density (kg/m ³)	26.28	21.65	24.94	24.11
IV Measured (L)	50.63	50.29	50.55	50.86
IV Avg. (L)		50.58		
IV Std. Dev. (L)		0.24		
Rel. Std. Dev. (%)		0.47		

* IV, Std. Dev., Rel., stand for internal volume, standard deviation, relative, respectively.

The volume measured of each section is the total volume of the system section, two expansion tanks, the sampling tank and piping in between. And average volume of those four repeated tests is calculated for each section. However, the volume used to

calculate R410A mass later in the steady-state test will subtract the sampling tank volume (5.9 L).

The relative standard deviations of measure internal volumes are 0.29% and 0.47% for outdoor unit section and liquid line section, respectively. However, the relative standard deviation is 1.15% for indoor unit plus vapor line section. One of the possible reason to cause the relatively large standard deviation is that the indoor unit was installed in a different room with the psychrometric chamber in which the expansion tanks were installed. And the long piping in between was exposed to the ambient environment which was only controlled by the room air conditioner so that larger variation of ambient temperature is expected than that controlled by the psychrometric chamber.

Nevertheless, even with the largest deviation of 1.15% and 2-sigma standard for uncertainty propagation, the uncertainty of those volume values is translated to the uncertainty of refrigerant mass and the uncertainty of refrigerant mass is expected to be at most 5%, which is quite accurate for obtaining the refrigerant charge distribution in each system section under steady-state condition.

4.3.2 Charge Sensitivity Test

Once the mass of vapor state refrigerant was calculated for each section, the refrigerant was recovered back to the system using a recovery compressor. However, there is a possibility that a small amount of refrigerant is trapped in the expansion tanks and piping since the recovery compressor is not able to evacuate the expansion system to a

deep vacuum. Therefore, to guarantee the system maintaining the same charge every time after the expansion process, a correlation between the system charge and system performance parameter needs to be developed and a compensation of system charge is needed.

The unit was tested under ASHRAE C condition with increasing R410A charge, and condenser outlet subcooling and condensing pressure were calculated and plotted versus system charge as shown in Figure 29. Five tests were repeated to obtain the correlations. As observed, the condenser outlet subcooling increases linearly with the increasing system charge and the condensing pressure increase quadratically with increasing charge. And both R-squared values are higher than 0.999, which shows the reliability of these correlations. Thus, with these two correlations, the system charge could be back calculated after every expansion process. If the system is under-charged,

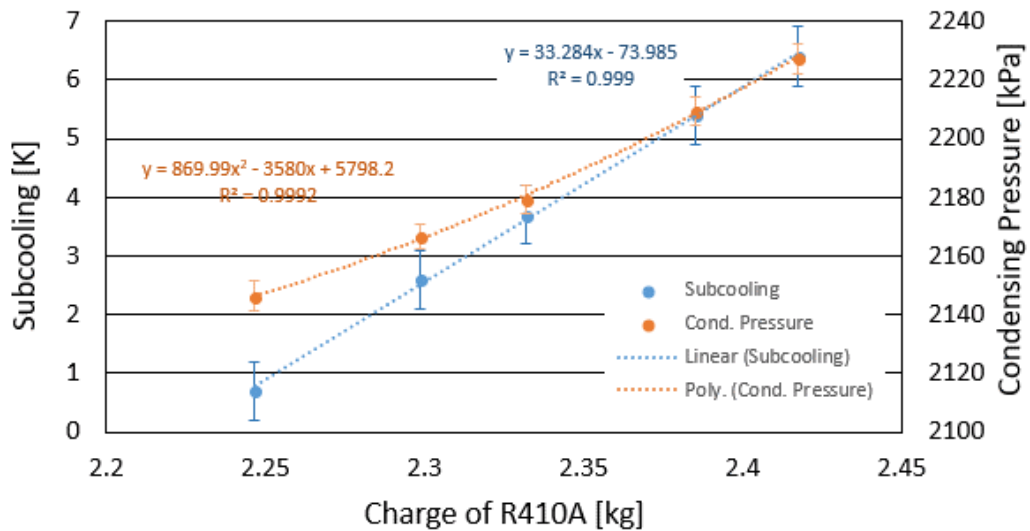


Figure 29: Correlations between Subcooling and Condensing Pressure with System Charge

an extra amount of refrigerant would be charged to compensate the amount of refrigerant trapped in the expansion system.

The correlation of outdoor unit power consumption and system charge is shown in Figure 30. The power consumption increases quadratically with the increasing system charge. All the linear and quadratic equations shown in Figure 29 and Figure 30 are fitted using Excel and the R values are shown below the equation formula.

Ideally, the compensation charge is only needed after the first time of expansion if the same stop criterion of recovery compressor is chosen. However, the system charge is checked with these correlations after every expansion process so that the total system charge could remain the same all the time. And the data of repeated charge distribution tests under steady-state conditions are reliable.

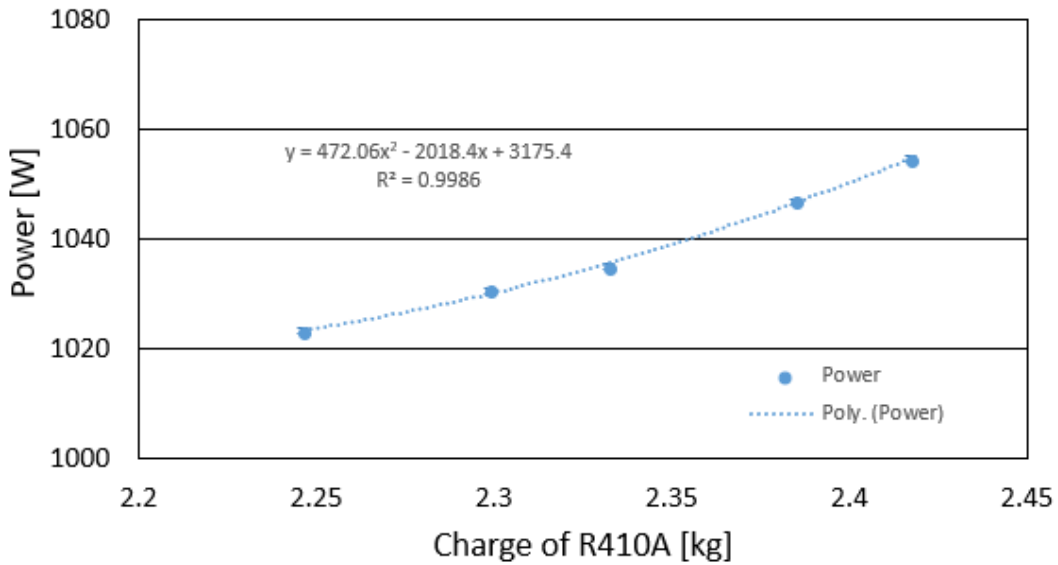


Figure 30: Correlations between Outdoor Unit Power Consumption with System Charge

4.3.3 Oil Monitoring

Since mass flow rate of refrigerant from the system components to the expansion tanks could be large and it carries compressor oil while expanding, especially for the liquid phase refrigerant, it is likely that the amount of compressor oil would decrease as the charge distribution tests being repeated since the compressor oil could be trapped in the tanks and piping of the expansion subsystem. Moreover, the recovery process may not be able to recover all the oil, and insufficient oil lubrication could adversely impact or even damage the scroll compressor. Therefore, a customized compressor with a sight tube is installed to monitor the oil level in the scroll compressor as shown in Figure 31.



Figure 31: The Scroll Compressor with a Sight Tube

A type of fluorescent dye for HVAC system was used to trace the oil in the sight tube since the clean oil is clear and hard to observe. The fluorescent dye was charged through the oil charging port as shown in the Figure 31. And the glowing oil under UV light is

shown in Figure 32. The black marked tick is to indicate the oil level quantitatively, the distance between large ticks is 0.0254 m and that between large tick and small tick is 0.0127 m. And the longest tick is the manufacturer-recommended oil level. The top of the glowing section is the actual oil level in the compressor oil sump. In addition, to eliminate the impact of heat loss through the brass fittings on both sides of the sight tube, they are properly insulated with rubber foam.

A webcam was installed in the outdoor unit enclosure, and a picture is taken every time before starting up the compressor in a series of charge distribution tests. As shown in Figure 33, the left and right pictures indicate the oil levels before and after one charge distribution test under ASHRAE C condition, respectively. It is easy to observe the oil level didn't decrease after one expansion measurement and even increase about 0.5 inch in the oil sump, which is because the oil is circulating and relocating in the whole



Figure 32: Compressor Oil Level under UV Light

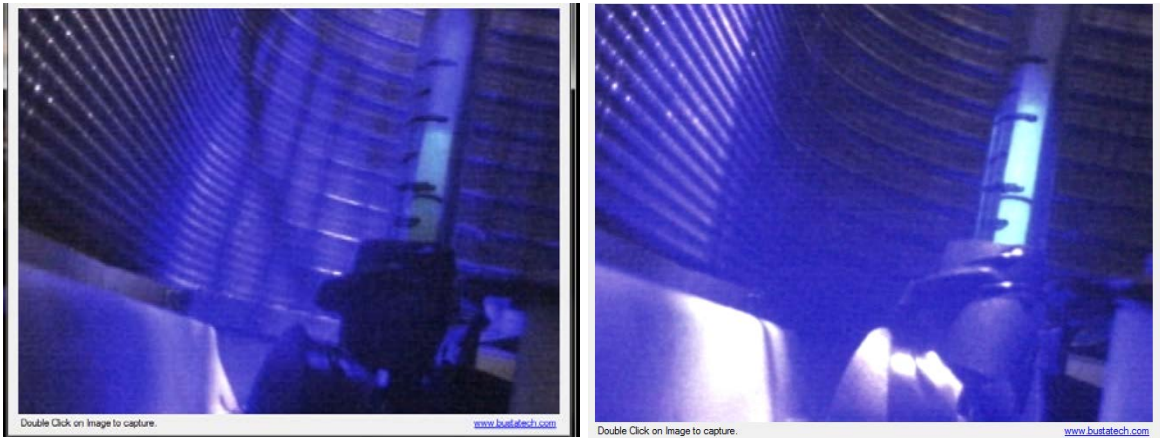


Figure 33: Oil Level under UV Light before (Left) and after One Charge Distribution Test (Right)

system as the expansion and recovery process going on and there is oil in the rotary compressor as well. After ten refrigerant charge distribution tests, the compressor oil was still above the required oil level and there is no significant change in oil level. Therefore, it is concluded that, for this experimental setup, we don't need to be worried about the oil migration and the compressor can work well with sufficient lubrication.

4.3.4 Charge Distribution Test Results

Refrigerant charge distribution tests have been carried out under ASHRAE A, B and C conditions, to make sure the repeatability of the results, at least three tests were repeated for each condition. The measured distribution results are shown in Table 13.

Although the time of expansion process is about 8 hours in the volume calibration test, the average time for the refrigerant stabilizing in the expansion process under steady-state conditions is only 1 hour and all three sections take the similar time for expansion.

Table 13: Refrigerant Charge Distribution under Steady-state Conditions

Parameter	ASHRAE A	Unc.	ASHRAE B	Unc.	ASHRAE C	Unc.
M_{ODU} (kg)	0.82	0.01	0.76	0.01	0.76	0.01
M_{Liq} (kg)	0.87	0.01	0.89	0.01	0.90	0.01
$M_{\text{IDU\&Vap}}$ (kg)	0.60	0.02	0.63	0.02	0.62	0.02
M_{Total} (kg)	2.29	0.03	2.28	0.03	2.28	0.03
$M_{\text{Dissolved}}$ (kg)			0.08			
M_{Charged} (kg)	2.40	-	2.40	-	2.40	-

The data shown in Table 13 are the average values from repeated tests for each section.

As we can see, there is a deviation between the total mass of refrigerant measured and the actual charge in the system, which can be justified by the amount of refrigerant dissolved in the compressor oil. The maximum amount of refrigerant dissolved in oil consists of the refrigerant dissolved in the scroll compressor and that in the rotary compressor for recovery. The oil solubility at certain temperature is found in Figure 34. Under ASHRAE C condition, the measured sump oil temperature is 40°C and suction pressure is 10 bars, from the chart below, it is easy to find the mass fraction of refrigerant dissolved in the POE 32 oil is 13%. Regarding the charged amount of the scroll compressor is 0.62 L, the maximum amount of refrigerant dissolved in the scroll compressor oil is 0.08 kg.

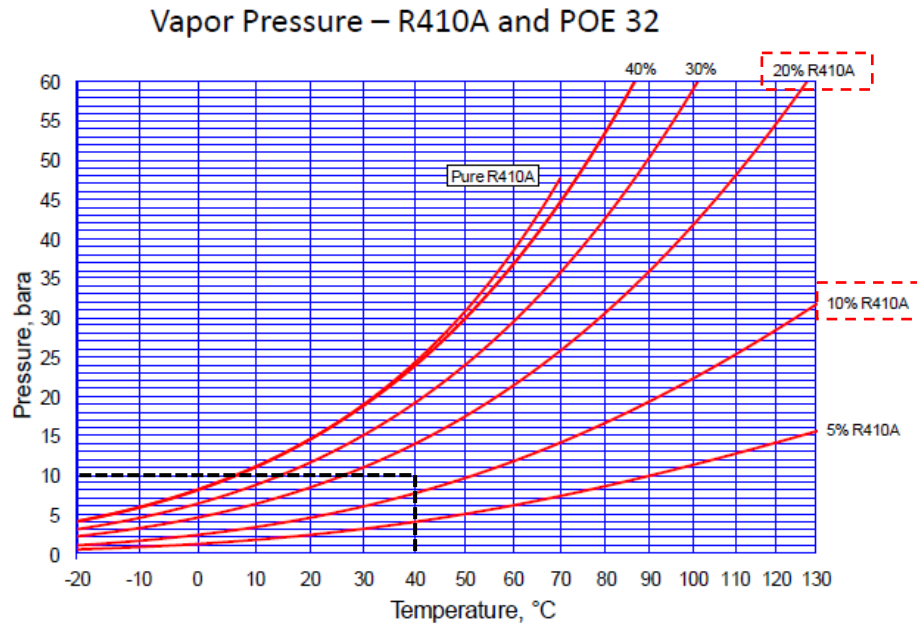


Figure 34: Vapor Pressure Correlation with Temperature of R410A and POE 32 Oil [35]

The amount dissolved in the rotary compressor was estimated based on the charged oil of 0.28L and the maximum amount of refrigerant was calculated to be 0.36 kg. In addition, to guarantee the rotary compressor work well with our AC system, an extra amount of 0.1 L POE oil was charged for compatibility. Thus, it is hard to numerically justify the amount of R410A dissolved in the rotary compressor oil. Nevertheless, with the maximum amount of 0.08 kg can dissolved in the scroll compressor oil and taking into account that the measurement uncertainty, the deviation between the total measured charge and the actual charge is justified. As shown in Figure 35, the charge difference between sections under steady-state conditions can be easily compared.

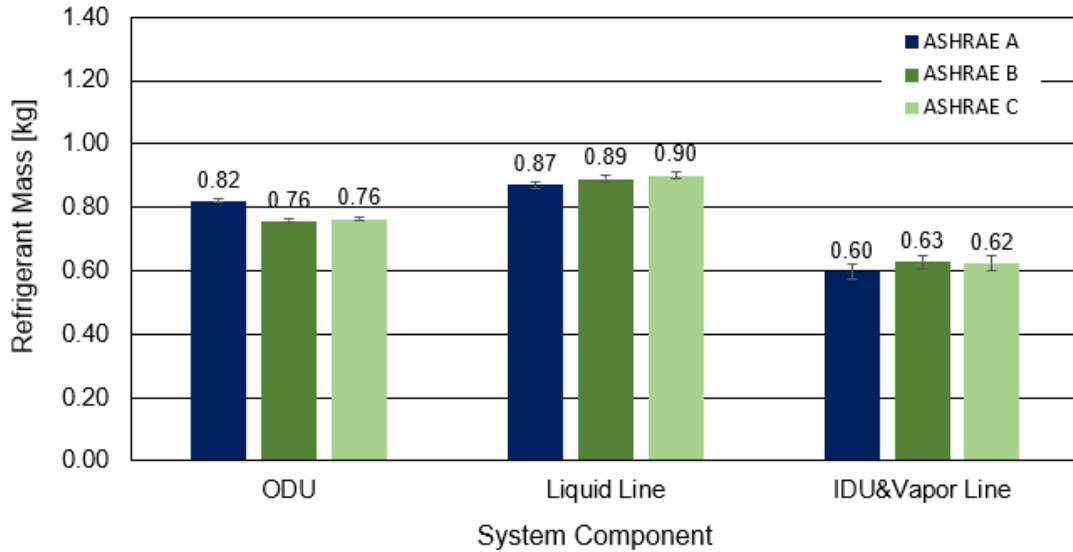


Figure 35: Charge Distribution of Steady-state Conditions Breakdown of Sections

Overall, as the test facility at UMCP has 10.67 m long piping connecting the indoor unit and outdoor unit with quite a large value of internal volume, the liquid line takes the most amount of refrigerant among all three sections under steady-state conditions, on the contrary, since most of the refrigerant in the indoor unit and vapor line piping is in vapor or two-phase, the indoor unit plus vapor line section takes the least amount of refrigerant. For the breakdown of sections, first, as the condenser outlet subcooling under ASHRAE A condition is the highest, the outdoor unit section holds more refrigerant than the other two conditions. Moreover, the ASHRAE B and C conditions have the same air temperature for both indoor and outdoor units, but the only difference is the inlet relative humidity at the indoor unit, which doesn't have effects on the charge in the outdoor unit. Thus, the charge of outdoor unit under B and C conditions are the same. For the liquid line section, since it only takes subcooled liquid, based on the pressure and temperature measured at the liquid line inlet and outlet, the liquid density

calculated out for ASHRAE A, B, and C conditions are 1000.3 kg/m³, 1032.9 kg/m³, 1037.3 kg/m³, respectively. It shows the same increasing trend for the charge in the liquid line section. As for the indoor unit section, the differences under different condition are within the range of uncertainty, so we cannot make any conclusion from the data.

Regarding the uncertainty calculation of charge distribution test, it is calculated based on the standard deviation of the results of internal volume calibration test. The relative standard deviation values in the volume calibration test are 0.29%, 0.47%, and 1.15% for outdoor unit, liquid line, and indoor unit plus vapor line section, respectively. And two-sigma standard is used for uncertainty propagation of measured refrigerant charge, specifically, the relative values of uncertainty of internal volume used to calculate the mass are 0.58%, 0.94%, and 2.3%, respectively. Moreover, the uncertainty of refrigerant vapor density is calculated from the uncertainty of measured pressure and temperature using Excel spreadsheets.

4.3.5 Results Comparison with Published Data

To validate the experimental results of this study, the measured refrigerant charge distribution results are compared to the published experimental results. However, as mentioned in the Chapter 2, there are a few papers experimentally investigating the refrigerant charge distribution in air conditioners. Moreover, they have different components from this study and different types of refrigerant as well as units of different capacity. Thus, it is difficult to make a fair comparison. Thus, the relative

refrigerant charge is compared instead of the absolute charge values. The system parameters and test conditions that are compared are specified in Table 14.

Table 14: Published Experimental Results of Refrigerant Charge Distribution

Author	Test Condition		Refrigerant	Charge (kg)	Capacity (kW)	Accumulator
	Indoor (°C)	Outdoor (°C)				
Mulroy, Didion [16]	26.6	27.7	R22	3.95	10	Yes
Ding [22]	27	35	R410A	1.98	7.1	Yes
Li [26]	27	35/27	R290	0.3	2.6	Yes
Li [30]	26	35	R410A	1.06	2.6	Yes

The results of refrigerant charge distribution in different system components under ASHRAE A and C conditions (outdoor unit temperature: 35°C and 27°C) are compared in Figure 36 and Figure 37, respectively. As we can observe, the refrigerant charge in

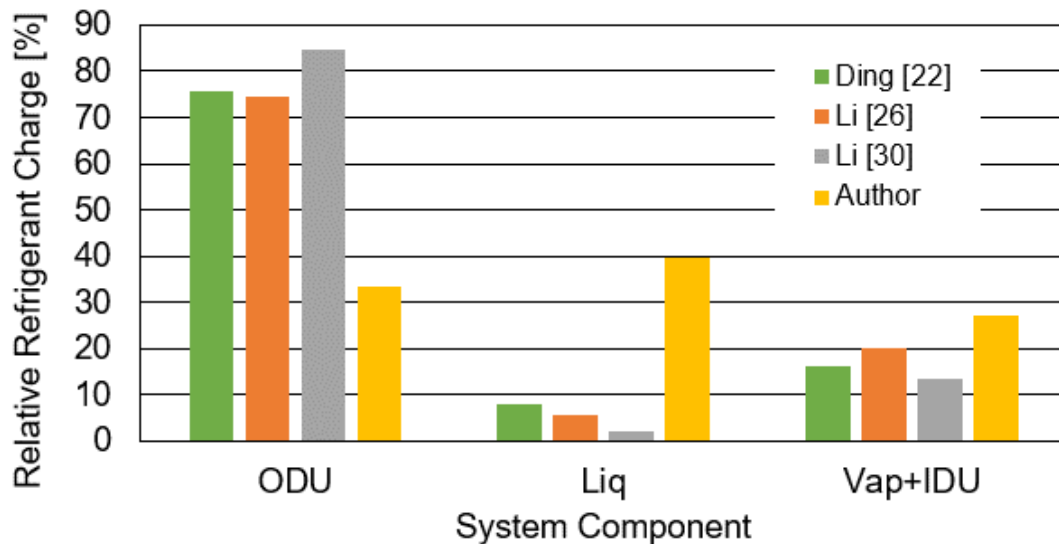


Figure 36: Refrigerant Charge Distribution under ASHRAE A Condition

different systems have quite different distributions. The systems of outdoor unit data in the published studies all include accumulators so that the relative value of refrigerant charge in the outdoor unit section of published papers are much higher than that of this study. Since the liquid line and vapor line piping at UMCP connecting the outdoor unit and indoor unit are 10.67 m long, which is much longer than every single case compared, the refrigerant charge in the liquid line of this study takes much higher amount of refrigerant, and so does the vapor line plus indoor unit section. However, it is noted that, from the results of Li [26] and of this study, we can find that the outdoor unit temperature does not have a drastic impact on the refrigerant charge distribution. In addition, it is too tedious and complicated to compare all the geometry parameters of each system component to justify the differences between those results of various systems charged with different types of refrigerant.

The refrigerant charge distribution results are compared with standard length of liquid line setup for the unit. And the comparisons are shown in Figure 38 and Figure 39.

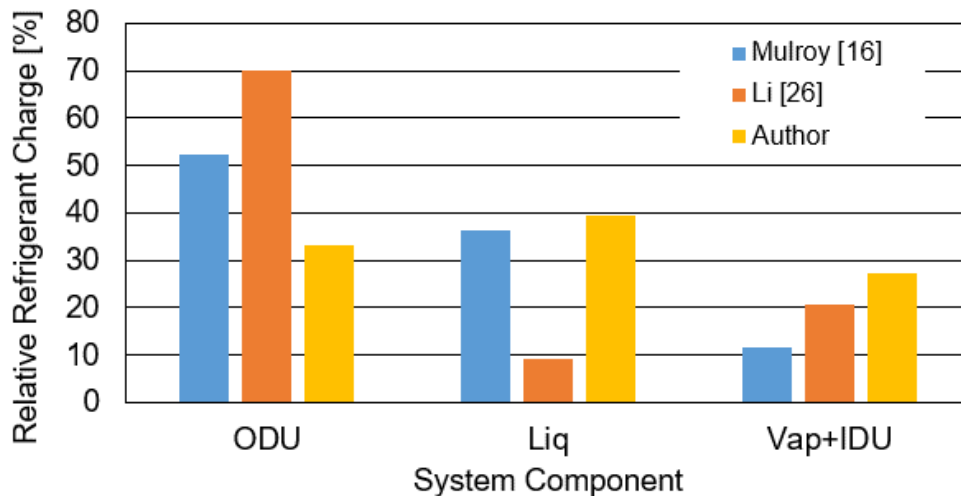


Figure 37: Refrigerant Charge Distribution under ASHRAE C Condition

To summarize, the refrigerant charge distribution highly depends on the factors including system component geometries and the design of the test setup. It is hard to directly compare the experimental results with the published results due to such differences in systems.

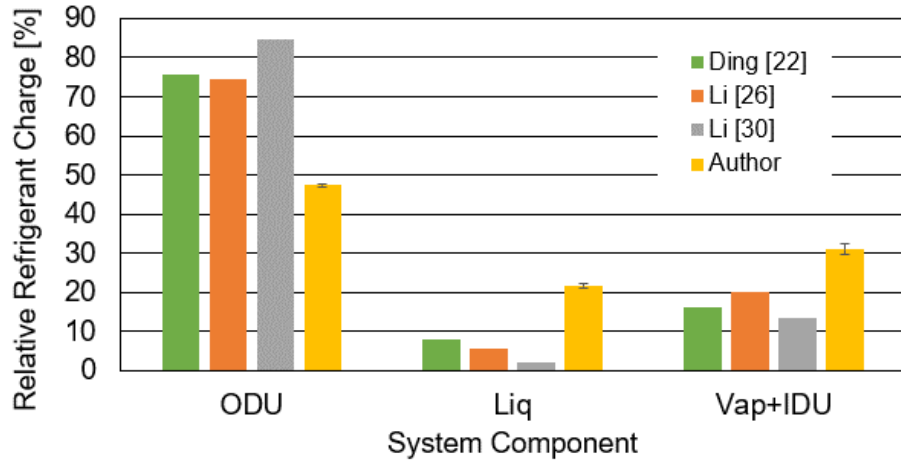


Figure 38: Refrigerant Charge Distribution under ASHRAE A Condition (Liquid Line Length Corrected)

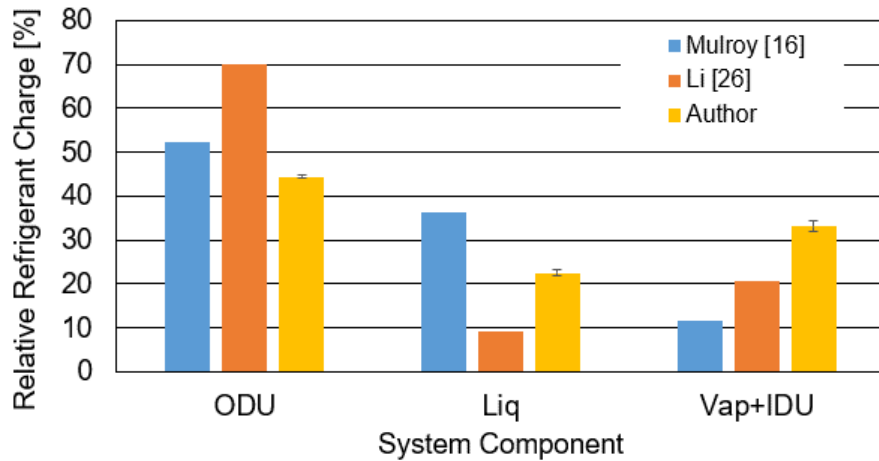


Figure 39: Refrigerant Charge Distribution under ASHRAE C Condition (Liquid Line Length Corrected)

Chapter 5 : Conclusions

In this study, a test facility that is able to carry out cyclic test of air-conditioning unit was built in CEEE heat pump lab. The baseline tests under ASHRAE standard test conditions A, B, and C and the cyclic test under ASHRAE D condition have been carried out. All the data have been analyzed and compared to manufacturer's specification and degradation coefficient has been evaluated. Furthermore, the system has been modified and an expansion subsystem has been added, by which a new approach proposed for refrigerant charge distribution measurement has been implemented. Refrigerant charge distribution inside system components has been studied under steady-state conditions (A, B and C). The main contributions of the study are summarized as follows:

- A customized code tester with a bypass duct that is parallel to the testing duct in which the indoor unit was installed was built up and four electrical dampers was installed to switch the airflow between testing duct during ON period and bypass duct during OFF period;
- The system performance of the unitary air-conditioning unit has been analyzed under steady-state conditions and all the data and system parameters including power consumption, cooling capacity and COP show a good match to the manufacturer's specifications;
- Cyclic performance of the unit has been tested and transient profiles of various system parameters measured have been plot. And transient cooling capacity and

power consumption during ON period has been calculated and degradation coefficient has been evaluated in the basis of integrated values of capacity and power consumption;

- The thermal mass of the code tester does influence the performance evaluation of air-conditioning units and it is of importance that the variables in the code tester such as thermal mass need to be normalized in the unit evaluation process;
- The expansion method for refrigerant charge measurement has been proposed and implemented. The internal volume of system components has been calibrated using pure refrigerant R134a. And refrigerant charge distribution tests under steady-state A, B, and C conditions have been measured and all the tests have been repeated to guarantee their reliability and repeatability. The liquid line section takes the most amount of refrigerant while the indoor unit plus vapor line section takes the least under all three steady state conditions, and it is hard to compare the experimental results with the published data due to the different system components and test setup.

Chapter 6 : Future Work

It is acknowledged that the transient system performance of air conditioning units highly depends on the test environment and experimental setup. The methodology and experimental setup for the unit rating tests of this study are both in accordance with the ASHRAE and AHRI standards to obtain a good understanding of the system and more reliable test data. However, from the experience of conducting steady-state and cyclic tests, the test facility could be further improved as follows to be more reliable and easily-controlled:

- 1) Testing duct of the code tester could be built longer: due to the height limitation of the test room, the leaving air stream of the indoor unit is not fully mixed, and it is observed a maldistribution at the leaving thermocouple grid. A longer straight testing duct before and after the indoor unit provides not only more accurate differential pressure measurement, but also enough space for mixing so that more accurate air leaving temperature could be measured;
- 2) Faster electrical-actuated dampers could be installed: the closing and opening time of the electrical dampers installed are 20 seconds and 60 seconds, respectively. To achieve instant switch of the air flow during the cyclic test, the two dampers at the inlet and outlet of the testing duct are controlled manually, which is tedious and problematic and could result in the inaccuracy of the timing to switch the air flow. Damper that could be actuated electrically and has a shorter response time could

significantly simplify the test procedures and reduce the human intervention on the test results;

- 3) Electrical shut-off valve could be installed: seven manual-controlled ball valves installed for the refrigerant expansion and recovery, which are cumbersome and complicated to manually switch those valves in the charge measurement tests. Electrically actuated shut-off valves could be installed to reduce the work load to carry out the charge distribution test;
- 4) Vacuum pump and refrigerant recovery integrated machine could be installed: the rotary compressor used to recover the refrigerant cannot achieve a deep vacuum and the residual of refrigerant needs to be calculated to correct the results of following expansion tests. A 2-in-1 integrated machine that could evacuate the expansion system could reduce the influence of the oil of rotary compressor and guarantee that all the refrigerant is recovered back to the system so that obtain a more straightforward calculation and more accurate charge measurement.

In addition, to acquire a more comprehensive understanding of the unit performance and more meaningful data presentation, more tests could be carried out as follows:

- 1) More quick closing valves could be installed: The system of this study is isolated into three sections in the charge measurement tests. The vapor line is included in the evaporator section and the compressor is included in the condenser section. Quick closing valves could be installed to separate those sections to obtain a more direct understanding of the system as, for instance, there is a pressure difference between the suction and discharge of the compressor. Isolating the compressor and

- the condenser coil could provide a more straightforward presentation of the refrigerant distribution with respect to low-pressure and high-pressure sides.
- 2) Thermal mass of the code tester could be altered: it is noted that the physical geometries of the code tester could influence the air-side capacity measurement. The sheet metal of duct sections, indoor unit case, mixer and so on store cooling capacity during ON period under the cyclic condition and cool down the air during OFF period, which could influence the evaluation of C_d . An experimental investigation of the effect of thermal mass of the code tester could be carried out by altering the thermal mass. It is practical to add thermal mass by adding metal cubes or water bags at the leaving duct of the indoor unit or install an electrical heater to act as a thermal load;
 - 3) Large capacity unit could be tested: another way to study the effect of the thermal mass of the code tester is to test units of different capacities to obtain a correlation between the cyclic degradation with the system capacity. Moreover, the effect of system capacity on the refrigerant charge distribution could also be investigated in those cases;
 - 4) Charge migration test could be carried out: the migration of refrigerant during cyclic operation is essential to the transient performance of AC units. With the test facility of this study, charge migration test under cyclic condition could be conducted to quantitatively investigate the effect of refrigerant charge inside system components on the transient performance.

Reference

- [1] UNEP, “Accelerating the Global Adoption of ENERGY-EFFICIENT AND CLIMATE-FRIENDLY AIR CONDITIONERS,” 2017.
- [2] “Global A/C Market Starting to Warm Up | 2014-08-18 | ACHRNEWS,” 2013. [Online]. Available: <https://www.achrnews.com/articles/127385-global-ac-market-starting-to-warm-up>.
- [3] Y. J. Hwang and H. Y. Kim, “Experimental and Theoretical Studies on the Transient Characteristics During Speed Up of Inverter Heat Pump,” *Int. Refrig. Air Cond. Conf.*, 1998.
- [4] M. Kim and C. W. Bullard, “Dynamic characteristics of a R-410A split air-conditioning system,” *Int. J. Refrig.*, vol. 24, pp. 652–659, 2001.
- [5] A. R. S. Kapadia, R. G., Jain Sanjeev, “Transient Characteristics of Split Air-Conditioning Systems Using R-22 and R-410A as Refrigerants of Split Air-Conditioning Systems Using R-22 and R-410A as Refrigerants,” *HVAC&R Res.*, vol. 9669, no. June 2013, pp. 37–41, 2017.
- [6] J. Wu, J. Lin, Z. Zhang, Z. Chen, J. Xie, and J. Lu, “Experimental investigation on cold startup characteristics of a rotary compressor in the R290 air-conditioning system under cooling condition,” *Int. J. Refrig.*, vol. 65, no. 28, pp. 209–217, 2016.
- [7] B. Li and A. G. Alleyne, “A dynamic model of a vapor compression cycle with shut-down and start-up operations,” *Int. J. Refrig.*, vol. 33, no. 3, pp. 538–552,

2010.

- [8] M. R. Kærn, W. Brix, B. Elmegaard, and L. F. S. Larsen, “Compensation of flow maldistribution in fin-and-tube evaporators for residential air-conditioning,” *Int. J. Refrig.*, vol. 34, no. 5, pp. 1230–1237, 2011.
- [9] G. Bagarella, R. M. Lazzarin, and B. Lamanna, “Cycling losses in refrigeration equipment: An experimental evaluation,” *Int. J. Refrig.*, vol. 36, no. 8, pp. 2111–2118, 2013.
- [10] J. Wu, J. Lin, Z. Zhang, Z. Chen, J. Xie, and J. Lu, “Experimental investigation of dynamic characteristics of a rotary compressor and its air conditioner using R290 during warm startup,” *Appl. Therm. Eng.*, vol. 125, pp. 1469–1477, 2017.
- [11] L. Cremaschi, Y. Hwang, and R. Radermacher, “Experimental investigation of oil retention in air conditioning systems,” *Int. J. Refrig.*, vol. 28, no. 7, pp. 1018–1028, 2005.
- [12] E. Fuentes, D. A. Waddicor, and J. Salom, “Improvements in the characterization of the efficiency degradation of water-to-water heat pumps under cyclic conditions,” *Appl. Energy*, vol. 179, pp. 778–789, 2016.
- [13] J. M. Corberan, D. Donadello, I. Martinez-Galv??n, and C. Montagud, “Partialization losses of ON/OFF operation of water-to-water refrigeration/heat-pump units,” *Int. J. Refrig.*, vol. 36, no. 8, pp. 2251–2261, 2013.
- [14] Jun Wang and Yezheng Wu, “Start-up and shut-down operation in a reciprocating compressor refrigeration system with capillary tubes,” *Int. J. Refrig.*, vol. 13, no. 3, pp. 187–190, 1990.

- [15] S. A. Tassou and P. Votsisi, "Transient Response and Cycling Losses of Air-to-water Heat Pump Systems," *Heat Recover. Syst. CHP*, vol. 12, no. 2, pp. 123–129, 1992.
- [16] W. J. Mulroy and D. A. Didion, "Refrigerant Migration in a Split-Unit Air Conditioner.," *ASHRAE Transactions*, vol. 91, no. pt 1A, pp. 193–206, 1985.
- [17] M. I. Belth, T. E. Grzymala, and D. R. Tree, "Transient mass flow rate of a residential air-to-air heat pump," *Int. J. Refrig.*, vol. 11, no. 5, pp. 298–304, 1988.
- [18] V. P. Sheth and T. A. Newell, "Refrigerant and Oil Migration and Retention in Air Conditioning and Refrigeration Systems," *Air Cond. Refrig. Cent.*, vol. 61801, no. 217, 2005.
- [19] E. Björk and B. Palm, "Refrigerant mass charge distribution in a domestic refrigerator, Part I: Transient conditions," *Appl. Therm. Eng.*, vol. 26, no. 8–9, pp. 829–837, 2006.
- [20] F. Poggi, H. Macchi-Tejeda, D. Leducq, and A. Bontemps, "Refrigerant charge in refrigerating systems and strategies of charge reduction," *Int. J. Refrig.*, vol. 31, no. 3, pp. 353–370, 2008.
- [21] S. Peuker and P. S. Hrnjak, "Refrigerant Mass and Oil Migration During Start-up Transient," *Int. Refrig. Air Cond. Conf.*, pp. 1–8, 2008.
- [22] G. Ding, X. Ma, P. Zhang, W. Han, S. Kasahara, and T. Yamaguchi, "Practical methods for measuring refrigerant mass distribution inside refrigeration system," *Int. J. Refrig.*, vol. 32, no. 2, pp. 327–334, 2009.

- [23] B. Li, S. Peuker, P. Hrnjak, and A. Alleyne, "Evaluation of Transient Refrigerant Migration Modeling Approach on Automotive Air Conditioning Systems," *SAE Int. J. Mater. Manuf.*, vol. 4, no. 1, pp. 2011-01-0649, 2011.
- [24] B. Li, S. Peuker, P. S. Hrnjak, and A. G. Alleyne, "Refrigerant mass migration modeling and simulation for air conditioning systems," *Appl. Therm. Eng.*, vol. 31, no. 10, pp. 1770-1779, 2011.
- [25] L. Palmiter, J. H. Kim, B. Larson, P. W. Francisco, E. A. Groll, and J. E. Braun, "Measured effect of airflow and refrigerant charge on the seasonal performance of an air-source heat pump using R-410A," *Energy Build.*, vol. 43, no. 7, pp. 1802-1810, 2011.
- [26] T. Li *et al.*, "Measurement of refrigerant mass distribution within a R290 split air conditioner," *Int. J. Refrig.*, vol. 57, no. 2010, pp. 163-172, 2015.
- [27] W. Tang, G. He, D. Cai, Y. Zhu, A. Zhang, and Q. Tian, "The experimental investigation of refrigerant distribution and leaking characteristics of R290 in split type household air conditioner," *Appl. Therm. Eng.*, vol. 115, pp. 72-80, 2017.
- [28] S. Jin and P. Hrnjak, "Refrigerant and lubricant charge in air condition heat exchangers: Experimentally validated model," *Int. J. Refrig.*, vol. 67, pp. 395-407, 2016.
- [29] L. Jierong and L. Tingxun, "Detailed dynamic refrigerant migration characteristics in room air-conditioner with R290," *Int. J. Refrig.*, vol. 88, pp. 108-116, 2018.

- [30] J. Li, W. Deng, and G. Yan, "Improving quick cooling performance of a R410A split air conditioner during startup by actively controlling refrigerant mass migration," *Appl. Therm. Eng.*, vol. 128, pp. 141–150, 2018.
- [31] ASHRAE, "Standard 116 Methods of Testing and Rating Seasonal Efficiency of Unitary Air Conditioners and Heat Pumps." p. 46, 1995.
- [32] ARI, "Standard 210/240 Performance Rating of Unitary Air-Conditioning and Air-Source Heat Pump Equipment," 2008.
- [33] ASHRAE, "Standard 37-2009 Rating Electrically Driven Unitary Air-Conditioning and Heat Pump," 2009.
- [34] R. Tillner Roth and H. D. Baehr, "An International Standard Formulation for the Thermodynamic Properties of 1,1,1,2-Tetrafluoroethane (HFC-134a) for Temperatures from 170 K to 455 K and Pressures up to 70 MPa," *J. Phys. Chem. Ref. Data*, 1994.
- [35] G. L. Smith, "Seminar 35 – Advances in Low Global Warming Potential (GWP) Refrigerants Refrigerant / Lubricant Properties of New Low GWP Options," *2014 ASHRAE Annu. Conf. Seattle*, pp. 1–26, 2014.